

95-7001
 November 1995
 (T/E)

Reevaluation of the Hadronic Contribution to $\alpha(M_Z^2)^*$

MORRIS L. SWARTZ

Stanford Linear Accelerator Center

Stanford University, Stanford, California, 94309

ABSTRACT

We reevaluate the hadronic part of the electromagnetic vacuum expectation value using the standard dispersion integral approach that utilizes the hadronic cross section measured in e^+e^- experiments as input. Previous analyses are based upon point-by-point trapezoidal integration which does not treat experimental errors in an optimal way. We use a technique that weights the experimental inputs by their stated uncertainties, includes correlations, and incorporates some refinements. We find the five-flavor hadronic contribution to the fractional change in the electromagnetic coupling constant at $q^2 = M_Z^2$, $\Delta\alpha(M_Z^2)$, to be 0.02752 ± 0.00046 , which leads to a value of the electromagnetic coupling constant, $\alpha^{-1}(M_Z^2) = 128.96 \pm 0.06$.

Submitted to *Physical Review D*

* Updated version of SLAC-PUB-6710. Work supported by Department of Energy, contract DE-AC03-76SF00515.

1. Introduction

At the current time, a large program of precise electroweak measurements is being conducted throughout the world. The object of this program is to test the electroweak Standard Model by comparing the measured values of a large set of electroweak observables with the predictions of the Minimal Standard Model (MSM). The Standard Model calculations have been performed to full one-loop accuracy and partial two-loop precision by a large community of researchers. In all of these calculations, it is necessary to evaluate the one-particle-irreducible contributions to the photon self-energy $\Pi_{\gamma\gamma}(q^2)$ or the related quantity $\Pi'_{\gamma\gamma}(q^2) \equiv (\Pi_{\gamma\gamma}(q^2) - \Pi_{\gamma\gamma}(0))/q^2$ at the Z mass scale $q^2 = M_Z^2$. These quantities are usually absorbed into the definition of the running electromagnetic coupling $\alpha(q^2)$,

$$\alpha(q^2) \equiv \frac{\alpha_0}{1 - [\Pi'_{\gamma\gamma}(q^2) - \Pi'_{\gamma\gamma}(0)]}, \quad (1)$$

where $\alpha_0 = 1/137.0359895(61)$ is the electromagnetic fine structure constant. This quantity is also represented as the fractional change in the electromagnetic coupling constant $\Delta\alpha$,

$$\Delta\alpha(q^2) = \frac{\alpha(q^2) - \alpha_0}{\alpha(q^2)} = \Pi'_{\gamma\gamma}(q^2) - \Pi'_{\gamma\gamma}(0). \quad (2)$$

Using analytic techniques and the optical theorem applied to the amplitude for s-channel Bhabha scattering, the quantity $\Delta\alpha$ has been related to the cross section for the process $e^+e^- \rightarrow \gamma^* \rightarrow \text{all}$ (σ_{tot}) as follows [1],

$$\Delta\alpha(q^2) = \frac{\alpha_0}{3\pi} P \int_{4m_e^2}^{\infty} ds \frac{q^2}{s(q^2 - s)} R_{tot}(s), \quad (3)$$

where $R_{tot}(s)$ is the ratio of the total cross section to the (massless) muon pair cross section $\sigma_{\mu\mu}(s) = 4\pi\alpha^2(s)/3s$ at the center-of-mass energy \sqrt{s} . The cross section σ_{tot} is the physical cross section which has been corrected for initial state radiation.

The actual quantity measured in most experiments is discussed in Appendix A. It should be noted in passing that equation (3) is correct to all orders in α_0 and relies only upon the assumption that the real part of $\Pi_{\gamma\gamma}$ is much larger than its imaginary part (the next-order correction is proportional to $\text{Im}^2\Pi_{\gamma\gamma}/|\Pi_{\gamma\gamma}|^2$ which is approximately 3×10^{-4} at $q^2 = M_Z^2$). It is straightforward to evaluate equation (3) for the continuum leptonic cross sections [2]. In the limit that the scale q^2 is much larger than the square of the lepton mass m_ℓ^2 , the contribution of the continuum leptonic cross sections is given by the following expression,

$$\Delta\alpha_\ell(q^2) = \frac{\alpha_0}{3\pi} \sum_\ell \left[-\frac{5}{3} + \ln \frac{q^2}{m_\ell^2} \right]. \quad (4)$$

The remaining contributions to R_{tot} consist of the continuum hadronic cross section and the $J^P = 1^-$ resonances and are labelled R_{had} . Since the cross sections for the resonances and low energy continuum are not accurately calculable from first principles, experimental inputs are used to evaluate their contributions equation (3). The contribution of open top quark production to the integral is accurately calculable and since the top quark mass is not known precisely, only the five flavor hadronic cross section is included in R_{had} . The corresponding contribution to $\Delta\alpha(q^2)$ is therefore,

$$\Delta\alpha_{had}(q^2) = \frac{\alpha_0}{3\pi} \text{P} \int_{4m_\pi^2}^{\infty} ds \frac{q^2}{s(q^2 - s)} R_{had}(s). \quad (5)$$

Equation (5) has been evaluated at the Z boson mass scale a number of times [3-8]. The most recent evaluations are by Martin and Zeppenfeld [6], Eidelman and Jegerlehner [7], and by Burkhardt and Pietrzyk [8] yield

$$\Delta\alpha_{had}(M_Z^2) = \begin{cases} 0.02739 \pm 0.00042, & \text{Reference 6} \\ 0.0280 \pm 0.0007, & \text{Reference 7} \\ 0.0280 \pm 0.0007, & \text{Reference 8.} \end{cases} \quad (6)$$

The authors of Reference 6 use perturbative QCD to parameterize the continuum $R_{had}(s)$ above $\sqrt{s} = 3$ GeV and linear interpolation of measured data below that

point. The two-body final states $\pi^+\pi^-$ and K^+K^- are fit to parameterizations which include the ρ , ω , and ϕ resonances. The remaining resonance contributions are calculated from an analytic expression which results from integrating a Breit-Wigner lineshape and depends upon the masses, widths, and leptonic widths of each resonance. The authors of Reference 7 use linear interpolation (trapezoidal integration) of measured data points to evaluate the continuum, $\pi^+\pi^-$, and K^+K^- contributions. Above $\sqrt{s} = 40$ GeV, they use perturbative QCD to evaluate R_{had} . The contributions of the ω , ϕ , J/ψ -family, and Υ -family resonances are included by integrating a Breit-Wigner lineshape. The authors of Reference 8 use smoothed averages of data to evaluate the continuum contribution, a parameterization to evaluate the $\pi^+\pi^-$ contribution, and the analytic expression to evaluate the contribution of the remaining resonances.

This document reports on an evaluation of equation (5) which is performed in a somewhat different way from those listed above. In particular, the technique employed makes better use of the information provided by the various R_{had} measurements, avoids some pitfalls inherent in the trapezoidal technique, and naturally provides an accurate estimate of the uncertainty on the result. We find

$$\Delta\alpha_{had}(M_Z^2) = 0.02752 \pm 0.00046,$$

which appears to be consistent with Refs. 6-8 within quoted errors.

The result reported here updates an earlier result [9] which was more discrepant with Refs. 6-8. The updated value of $\Delta\alpha_{had}(M_Z^2)$ is larger than the previous one by 8.6×10^{-4} for five reasons. The previous analysis used the six-flavor definition of $\Delta\alpha_{had}$ which differs from the five-flavor quantity by 0.6×10^{-4} . A (hopefully) less controversial choice of $\alpha_s(M_Z^2)$ shifts the result by -0.5×10^{-4} . The fitting procedure used in the previous analysis was biased toward smaller R_{had} values; correction of this problem gives a difference of 2.9×10^{-4} . Small corrections to the analysis of the resonant contribution change the result by -0.1×10^{-4} . But, the largest change is caused by the incorporation of a precise, new measurement of

R_{had} near charm threshold which alters the result by 5.8×10^{-4} . Although the net result is somewhat closer to those given above, a detailed comparison of the actual integrated cross section with one used in a trapezoidal integration (see Section 2.7) indicates that significant differences persist.

2. The Analysis

Any attempt to combine the results of many experiments is a perilous undertaking. Many different techniques and approaches have been used. Not all researchers have addressed all possible problems nor are systematic error estimates performed in uniform ways or to uniform standards. We therefore adopt some the techniques of the Particle Data Group [10]. Older measurements which are contradicted by newer, more precise work are excluded from the analysis. Parameter uncertainties that are extracted from fits with χ^2 per degree of freedom (dof) larger than one are rescaled by the factor $\sqrt{\chi^2/dof}$.

2.1 ANALYSIS TECHNIQUE

The experimental measurements of $R_{had}(s)$ are performed over limited regions of $W \equiv \sqrt{s}$. Typically, an experimental result consists of several points $R_{had}^i = R_{had}(W_i)$ measured at closely spaced energy points W_i . Each set of measurements is accompanied by a set of point-to-point uncertainties (statistical and systematic) $\sigma_i(\text{ptp})$ and an overall normalization uncertainty $\sigma(\text{norm})$. Quite often, the point-to-point uncertainties are much smaller than the normalization uncertainty. *A typical experimental result therefore consists of an accurately measured shape of less certain normalization.* In this case, the values of the measured points are strongly intercorrelated. For future reference, we label these as Type I correlations.

The normalization uncertainties usually incorporate purely detector-related effects, acceptance uncertainties, and uncertainties on radiative corrections and background corrections. The largest normalization uncertainties (15-20%) are associated with the oldest measurements of R_{had} in the $W = 1-5$ GeV region. These

experiments typically had limited acceptance which when combined with a (common) limited understanding of the event structure lead to large uncertainties in the overall detection efficiencies. *The normalization errors associated with different sets of measurements performed at similar energies and times may be strongly correlated.* These correlations are distinct from those discussed above (which must be present) and are labelled as Type II correlations. When combining the results of separate experiments, one must be careful to include the possible presence of Type II correlations in a conservative estimate of the overall experimental uncertainty.

Most previous analyses of $\Delta\alpha_{had}$ evaluate various contributions to equation (5) by performing a trapezoidal integration with measured values of R_{had} . Different data sets are combined by weighting nearby points by the quadrature sums of their point-to-point and normalization uncertainties (assuming that all points are uncorrelated). The effects of possible Type II correlations on the overall uncertainty are accounted for differently in different analyses. Eidelman and Jegerlehner [7] sum the uncertainties associated with each point linearly. Burkhardt and Pietrzyk [8] and most of the earlier analyses assign typical normalization uncertainties to various intervals in W and sum the corresponding uncertainties on $\Delta\alpha_{had}$ in quadrature. The use of trapezoidal integration has two advantages: it is unbiased by human prejudice about the functional form of $R_{had}(s)$, and it would automatically account for undiscovered resonances which are broad as compared with the spacing of measurements. Unfortunately, this technique also has a serious shortcoming: it ignores the Type I correlations present in each data set.

Treating the combined (normalization and point-to-point) uncertainties on the points in each set as independent loses the (often precise) shape information associated with the set. Two examples of the loss of shape information are illustrated Figure 1. In part a), a data set with small point-to-point errors (shown as solid dots) and a large normalization uncertainty (illustrated to the right of the data) is combined with a single precise measurement (shown as the open dot). The statistical averaging procedure used in the trapezoidal integrations would yield the

function shown as the solid curve. The shape defined by the solid dots would be distorted near the single precise point and the accurate normalization information contained in the single measurement would be ignored. An more optimal procedure would use the shape information provided by the solid dots and the normalization information provided by the open dot yielding the dashed curve.

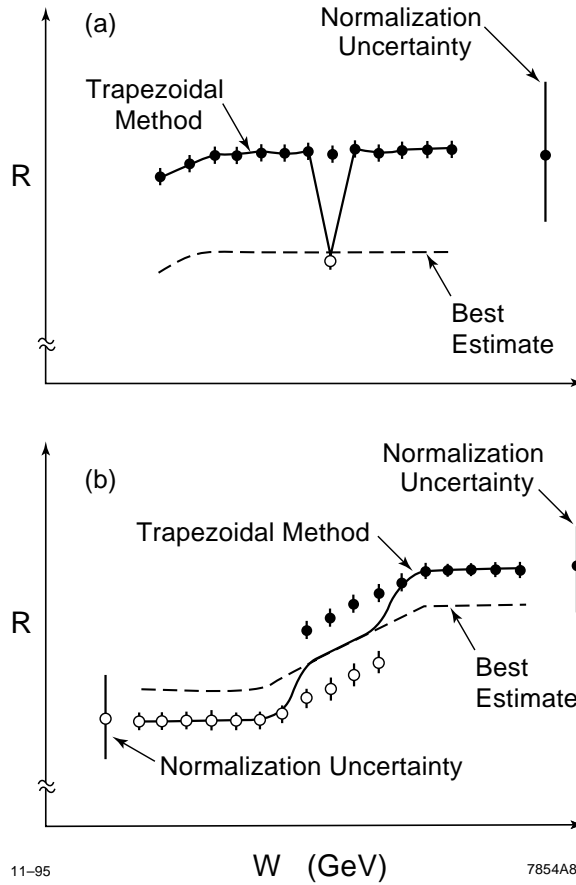


Figure 1. Two examples of the shape information loss inherent in the averaging procedures used by trapezoidal analyses.

Part b) of Figure 1 shows the result of combining two partly overlapping sets which have small point-to-point uncertainties and large normalization uncertainties (shown as open and solid dots, respectively). In the region of overlap, the sets define a consistent shape but differ in normalization. An optimal averaging procedure

would average the normalizations and produce the dashed curve. The procedure adopted as part of the trapezoidal analyses would yield the solid curve which agrees with the dashed one only in the region of overlap and does not preserve the shape determined by the data sets. The trapezoidal analyses described in References 4, 5, and 7 are checked by first integrating individual data sets and then by averaging the integrals. While it might appear that this procedure preserves shape information, the actual averaging of the integrals can be carried out only in energy intervals where the data sets overlap. The net result therefore looks much like the solid curve in part b). It is not surprising that consistent results were obtained. Optimal use of the shape information can occur only in techniques that allow the normalizations of the data sets to vary. The consequences of these examples will become clearer in Section 2.7.

We incorporate correlations into the analysis by fitting the data to an appropriate functional form $R_{fit}(s; a_k)$ where a_k are the parameters of the function. In the absence of undiscovered resonances, R_{had} can be described by a continuous function. A χ^2 fit has the virtue that measurements can be weighted by their experimental errors and correlations are straightforward to include. The previous version of this analysis used a non-diagonal definition of χ^2 constructed from the covariance matrix $E_{ij} = \langle \Delta R_{had}^i \Delta R_{had}^j \rangle$ of the measured points R_{had}^i . Unfortunately, it has been shown that if the off-diagonal elements E_{ij} scale with the measured values of R_{had}^i or R_{had}^j , the resulting fit will be biased to smaller values of R_{had} [11]. The bias that resulted to our previous analysis [9] from the application of the incorrect technique was approximately 39% of the uncertainty on the final result. We avoid the bias by defining χ^2 as follows,

$$\chi^2 = \sum_i \frac{[R_{had}^i - (1 + \lambda_j \alpha_i) R_{fit}(s_i; a_k)]^2}{\sigma_i^2(\text{ptp})} + \sum_j \lambda_j^2, \quad (7)$$

where R_{had}^i is the value of R_{had} measured at energy s_i , $\alpha_i = \sigma_i(\text{norm})/R_{had}^i$ is the fractional normalization uncertainty associated with the i^{th} measurement, and λ_j are fit parameters which are constrained to have zero mean and unit width. This

form preserves shape information and propagates the normalization uncertainties into the parameters of the function R_{fit} . For each fit, two choices of the parameters λ_j are investigated. In the first case, a separate normalization parameter λ_j is assigned to each data set. This choice incorporates Type I correlations only and makes no assumptions about correlations between experiments. In the second case, the normalizations of experiments of similar age and energy region are assumed to be 100% correlated. A separate normalization parameter is assigned to each correlated group instead of each set of measurements. This choice includes the effects of Type I and Type II correlations, produces larger error estimates (a consequence of including the Type II correlations), and is the one quoted as the *official* result. The difference in $\Delta\alpha_{had}$ resulting from the two weighting schemes is included in the parameterization uncertainty discussed below.

Equation (5) is evaluated by performing a Simpson's Rule integration using the function R_{fit} and the best estimate of the parameters. The parameter uncertainties δa_k reflect the point-to-point and normalization uncertainties to some extent. Unfortunately, the process of fitting a large number of measurements with a function of a smaller number of parameters necessarily involves some loss of information. The resulting uncertainty on the fitting function at some point W is usually smaller than the uncertainties on nearby data points. If we add *a priori* information to the problem by choosing a physically motivated fitting function, the information contained in the parameter error matrix may be appropriate. To understand this problem better, we evaluate the uncertainty on $\Delta\alpha_{had}(M_Z^2)$ by two techniques. In the first, the parameter uncertainties are propagated to the calculated value of $\Delta\alpha_{had}(M_Z^2)$ using the following expression which is valid for any function of the parameters,

$$\delta^2(\Delta\alpha_{had})_{exp} = \sum_{k,l} \frac{\partial(\Delta\alpha_{had})}{\partial a_k} E_{kl} \frac{\partial(\Delta\alpha_{had})}{\partial a_l}, \quad (8)$$

where the derivatives are calculated numerically and $E_{kl} = \langle \delta a_k \delta a_l \rangle$ is the parameter error matrix that is extracted from the fitting procedure. The second error

estimate is performed by constructing a large ensemble of data sets by shifting the measured data points $R_{had}^i(\text{meas})$ as follows,

$$R_{had}^i(\text{set } j) = R_{had}^i(\text{meas}) + f_{ij}^{\text{ptp}}\sigma_i(\text{ptp}) + f_{ij}^{\text{norm}}\sigma_i(\text{norm}), \quad (9)$$

where the factors f_{ij} are Gaussian-distributed random numbers of unit variance. The entire fitting and integration procedure is then applied to each member of the ensemble. The uncertainty on $\Delta\alpha_{had}(M_Z^2)$ is determined from the central 68.3% of the ensemble distribution.

The use of a fitting function has the problem that one may introduce bias through the choice of parameterization. We attempt to evaluate this effect by varying the parameterizations as much as ingenuity and computer time allow. The quoted contributions to $\Delta\alpha_{had}(M_Z^2)$ are those corresponding to the best fits. Each contribution is assigned a parameterization uncertainty $\delta(\Delta\alpha_{had})_{\text{param}}$ based upon the spread of results corresponding to reasonable fits. The parameterization uncertainty also includes a contribution from the difference observed in the two χ^2 weighting schemes.

2.2 THE DATA

The approach to the evaluation of equation (5) is driven by the form of the data themselves. The total hadronic cross section can be decomposed into four pieces: the hadronic continuum above $W \equiv \sqrt{s} = 1$ GeV, the charged two-body final states $\pi^+\pi^-$ and K^+K^- from their respective thresholds to 2.6 GeV, and hadronic resonances (excluding charged two-body final states). Since equation (5) is linear in the hadronic cross section, we decompose $\Delta\alpha_{had}$ as follows,

$$\Delta\alpha_{had}(q^2) = \Delta\alpha_{had}^{\text{cont}}(q^2) + \Delta\alpha_{had}^{\pi^+\pi^-}(q^2) + \Delta\alpha_{had}^{K^+K^-}(q^2) + \Delta\alpha_{had}^{\text{res}}(q^2), \quad (10)$$

where the four terms on the right-hand side correspond to the four pieces of the hadronic cross section.

The rationale for this decomposition is as follows. The region below $W = 1$ GeV is dominated by the ρ , ω , and ϕ resonances. The electromagnetic form factors for the processes $e^+e^- \rightarrow \pi^+\pi^-$ [12-19] and $e^+e^- \rightarrow K^+K^-$ [19-23] are measured well from threshold to $W \simeq 2$ GeV. Resonances do not account for all of the $\pi^+\pi^-$ and K^+K^- cross section in this region. On the other hand, essentially all other two-body and three-body final states are associated with the resonances. Measurements of three-pion final states near $W = 1$ GeV [24] show the non-resonant portion to be consistent with zero. Similarly, measurements of various two-body final states such as $K_L^0 K_S^0$ show small non-resonant cross sections [21]. The cross sections for four-pion final states become significant above 1 GeV but are small below that energy [25]. The $\gamma\gamma 2$ experiment [26] at the ADONE storage ring at Frascati has measured the hadronic cross section ratio for three or more hadron final states, $R_{had}^{\geq 3}$ from $W = 1.42$ GeV to $W = 3.09$ GeV. They have also presented several points from 1 GeV to 1.4 GeV that are composed of various multipion cross sections from Novosibirsk and Orsay [25,24,27] and are claimed to approximate $R_{had}^{\geq 3}$. Measurements beginning at $W = 2.6$ GeV by the MARK I [28], DASP [29], PLUTO [30], and Crystal Ball [31] Collaborations claim to measure the entire cross section. We therefore conclude that R_{had} is well approximated below $W_1 = 2.6$ GeV by a sum of the $\pi^+\pi^-$ and K^+K^- contributions from threshold to W_1 (where they are much smaller than $R_{had}^{\geq 3}$); the $R_{had}^{\geq 3}$ measurements from 1 GeV to W_1 ; and the ρ , ω and ϕ resonances where the hadronic widths are adjusted to remove the $\pi^+\pi^-$ and K^+K^- final states that are already included explicitly. Note that the several broad e^+e^- resonances between the $\phi(1020)$ and $W = 2$ GeV are implicitly contained in the two-body or $R_{had}^{\geq 3}$ categories. Since the $\pi^+\pi^-$ and K^+K^- cross sections are very small at W_1 , the $R_{had}^{\geq 3}$ and total continuum R_{had} measurements should be continuous at this point.

At center-of-mass energies larger than W_1 , many measurements of the hadronic continuum and resonances exist. The only precise measurement in the region between 2.6 GeV and 5.0 GeV is a single data point just below charm threshold at $W = 3.670$ GeV by the Crystal Ball Collaboration [31]. This measurement has a

normalization uncertainty of 7%. Since the next most precise measurements in the region below 5 GeV have normalization uncertainties of 15%, this measurement represents an important constraint on the magnitude of the cross section in the entire region. The region above charm threshold from $W = 3.77$ GeV to $W = 5.0$ GeV is complicated and not well measured. The MARK I, DASP, PLUTO and Crystal Ball Collaborations all observe an enhancement beyond the expected threshold shape. The DASP data show three resolved resonances. The MARK I and PLUTO data are consistent with the DASP data but do not cleanly resolve the resonances. The Crystal Ball measurements are somewhat smaller than the older ones and do not resolve the second resonance (which appears as a broad shoulder). We choose to follow the Particle Data Group and recognize the DASP resonances: $\psi(4040)$, $\psi(4160)$, and $\psi(4415)$. The ψ family therefore consists of six states.

Between 5 GeV and 10.4 GeV, the MARK I, DASP, PLUTO, Crystal Ball [32], LENA [33], CLEO [34], CUSB [35], and DESY-Heidelberg [36] Collaborations have published R_{had} measurements which are plotted in Figure 2. The error bars include only point-to-point uncertainties. The recently published Crystal Ball measurements have a systematic normalization uncertainty of 5.2%. The other measurements have normalization uncertainties in the range 6.8-10%. The data are also compared with the recent QCD prediction of Chetyrkin and Kuhn [37] which includes quark mass effects. At $W = 5$ GeV, the MARK I data are consistent with other measurements. As W increases, they show a systematic increase in R_{had} and suggest the presence of a structure near 6.6 GeV. Including the quoted 10% normalization uncertainty, the MARK I data are larger than the more precise measurements by approximately two standard deviations. The reader is reminded that first generation detectors like MARK I, DASP, and PLUTO were small acceptance devices that necessarily involved large acceptance corrections without the benefit of good event structure modelling. After acceptance corrections and a τ -lepton subtraction, the MARK I group observed that two-charged-prong events constituted nearly 20% of the hadronic cross section of R at $W = 7$ GeV. This is about 1.5 times the two-prong rate due to $\tau^+\tau^-$ final states and three times the rate that is

predicted [38] by the JETSET 7.3 Monte Carlo program [39]. While this may not be wrong, we choose to exclude data from the first generation experiments when more modern results are available. Such data are available above charm threshold. Unfortunately, we are constrained to use very old continuum measurements below charm threshold.

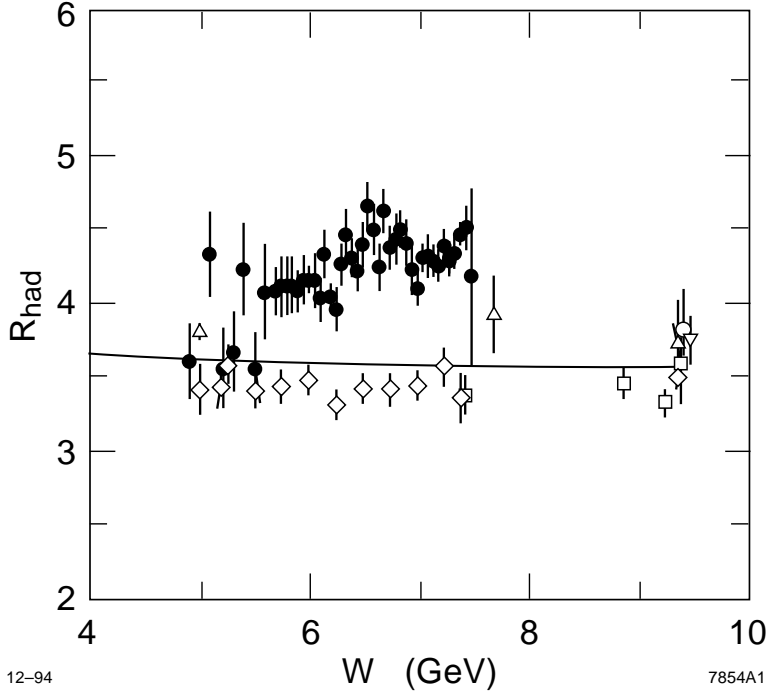


Figure 2. The R_{had} measurements of the MARK I [28] (solid squares), PLUTO [30] (open triangles), Crystal Ball [32] (open diamonds), LENA [33] (open squares), DASP [29] (open inverted triangle), and DESY-Heidelberg [36] (open circle) Collaborations in the region between $W = 5$ GeV and $W = 9.4$ GeV. The error bars include point-to-point uncertainties only. A recent QCD calculation [37] which includes quark mass effects is shown as a solid line for $\alpha_s(M_Z^2) = 0.125$.

The Particle Data Group lists six Υ family resonances between 9.4 GeV and 11 GeV. All are included in the resonance contribution.

Above b-quark threshold, a number of R_{had} measurements have been carried out by the PEP and PETRA experiments [40-45]. However at energies above

$W = 34$ GeV, Z - γ interference becomes significant. We therefore use only those measurements in the region $W \leq 34$ GeV where the correction for electroweak interference is less than 1%.

We expect that R_{had} is well described by perturbative QCD in the region above b-quark threshold. This implies that the world average value of the strong coupling constant $\alpha_s(M_Z^2)$ compiled by the Particle Data Group [10] provides a precise measurement of R_{had} at $W = M_Z$. Since possible anomalies in the Z lineshape would bias the determination of $\alpha_s(M_Z^2)$ from the lineshape parameters, we exclude the Z lineshape information from the Particle Data Group average. Additionally, since we explicitly include the PEP/PETRA R_{had} measurements in our fit (which uses perturbative QCD to describe the PEP/PETRA energy region), they are also excluded from the PDG average yielding the following value,

$$\alpha_s(M_Z^2) = 0.116 \pm 0.005. \quad (11)$$

To convert $\alpha_s(M_Z^2)$ into a determination of $R_{had}(M_Z)$, we use the third-order QCD expression [46],

$$R_{QCD}(s) = 3 \sum_f Q_f^2 \beta_f \frac{(3 - \beta_f^2)}{2} \cdot \left\{ 1 + \left[\frac{\alpha_s(s)}{\pi} \right] + r_1 \left[\frac{\alpha_s(s)}{\pi} \right]^2 + r_2 \left[\frac{\alpha_s(s)}{\pi} \right]^3 \right\}, \quad (12)$$

where: Q_f is the final state fermion charge, $\beta_f = \sqrt{1 - 4m_f^2/s}$ is the fermion velocity in the e^+e^- center-of-mass frame (m_f is the fermion mass), and the coefficients are functions of the number of active flavors N_f ,

$$r_1 = 1.9857 - 0.1153N_f$$

$$r_2 = -6.6368 - 1.2002N_f - 0.0052N_f^2 - 1.2395 \frac{(\sum Q_f)^2}{3 \sum Q_f^2}. \quad (13)$$

The resulting value of $R_{had}(M_Z)$ is,

$$R_{had}(M_Z) = 3.807 \pm 0.006. \quad (14)$$

The following three sections of this chapter describe the evaluation of: the continuum contribution $\Delta\alpha_{had}^{\text{cont}}$, the contributions of the charged two-body final states $\Delta\alpha_{had}^{\pi^+\pi^-}$ and $\Delta\alpha_{had}^{K^+K^-}$, and the resonance contribution $\Delta\alpha_{had}^{\text{res}}$.

2.3 THE HADRONIC CONTINUUM

The first step in the evaluation of equation (5) for the hadronic continuum is to formulate a suitable (piecewise-continuous) parameterization $R_{fit}(s; a_k)$. We choose to use the perturbative QCD expression given in equation (12) in the region $W \geq 15$ GeV and an empirical parameterization in the region $1 \text{ GeV} \leq W < 15$ GeV. In the high energy region, the only free parameter is $\alpha_s(M_Z^2)$ which is evolved to other scales numerically using the Runge-Kutta method applied to the order- α_s^4 renormalization group equation [47].

In the portions of the low energy region that are measured well, polynomials are used to parameterize $R_{had}(W)$. To ensure that the function is continuous across several points W_a , the polynomials are constructed in $x_a \equiv W - W_a$ and the zeroth order terms are excluded,

$$P_n^a(x) \equiv \sum_{i=1}^n d_i^a x_a^i, \quad (15)$$

where a is a label to distinguish different regions. Separate polynomials are used to describe the following regions: $1 \text{ GeV} \leq W \leq 1.9 \text{ GeV}$ (labelled region s), $1.9 \text{ GeV} < W \leq 3.6 \text{ GeV}$ (labelled region c), and $5.0 \text{ GeV} < W \leq 10.4 \text{ GeV}$ (labelled region b). Although a single, large-order polynomial is adequate to describe the data between $W = 1$ GeV and charm threshold at 3.6 GeV, the data show a distinct shape change near $W = 1.9$ GeV (where the four-pion cross section is becoming small). It was possible to obtain better fits by introducing an additional

polynomial to describe the region from 1 GeV to 1.9 GeV. A comparison of the two possible forms is used to assess the parameterization sensitivity of the final result.

Since there are no measurements of the continuum R_{had} in the b-quark and c-quark threshold regions (published measurements include a mixture of continuum and resonances), it is necessary to extrapolate the form of R_{had} from 3.6 GeV to 5.0 GeV and from 10.4 GeV to 15 GeV with functions that are physically motivated. In the case of the charm threshold region, the DASP Collaboration has published (in graphical form) the shape of the continuum that was preferred by their fit to the $\psi(4040)$, $\psi(4160)$, and $\psi(4415)$ resonances. The function which characterizes the shape of the threshold, $f_{DASP}(W)$, does not increase as sharply as the free-quark threshold factor $\beta(3 - \beta^2)/2$ but increases more rapidly than the β^3 threshold factor for pointlike scalar particles. To construct the function R_{fit} , all three possibilities are used for the c-quark threshold and the two extreme possibilities are used for the b-quark threshold,

$$f_c(W) = \begin{cases} \beta(3 - \beta^2)/2 \\ f_{DASP}(W) \\ \beta^3 \end{cases} \quad f_b(W) = \begin{cases} \beta(3 - \beta^2)/2 \\ \beta^3, \end{cases} \quad (16)$$

where the c- and b-quark masses are taken to be the D and B meson masses, respectively. The actual size of the charm-associated step in R_{had} , ΔR_c is left as a free parameter. The size of the bottom-associated step in R_{had} is constrained to be the difference between the value of the fit function at $W = 10.4$ GeV and the value of the QCD portion at $W = 15$ GeV, $\Delta R_b \equiv R_{QCD}(15) - R_{fit}(10.4)$.

The actual form of the fitting function is given by the following expression,

$$R_{fit}(W) = \begin{cases} R_0 + P_{N_s}^s(W - 1.0), & 1 \leq W \leq 1.9 \\ R_{fit}(1.9) + P_{N_c}^c(W - 1.9), & 1.9 < W \leq 3.6 \\ R_{fit}(3.6) + \Delta R_c f_c(W), & 3.6 < W \leq 5.0 \\ R_{fit}(5.0) + P_{N_b}^b(W - 5.0), & 5.0 < W \leq 10.4 \\ R_{fit}(10.4) + \Delta R_b f_b(W), & 10.4 < W < 15.0 \\ R_{QCD}(W), & 15 \leq W \end{cases} \quad (17)$$

where R_0 , the value of R_{had} at $W = 1$ GeV, is a free parameter and the order of the polynomials is varied from 1 to 7. The χ^2 is constructed from equation (7) assuming that normalization uncertainties are completely correlated in four groups: the 20% uncertainties of the lowest energy measurements [26-27] ($1.0 \text{ GeV} < W < 3.09 \text{ GeV}$), the 15-20% uncertainties of the MARK I, DASP, and PLUTO measurements [28-30] ($2.6 \text{ GeV} < W < 4.9 \text{ GeV}$), the 5-10% uncertainties of the measurements [32-36] between charm and bottom thresholds (the Crystal Ball measurement at 3.670 GeV is treated as a member of the higher-energy Crystal Ball set), and the 1.7-7.0% uncertainties of the PEP and PETRA experiments [40-45] above bottom threshold. Each fit is repeated with a separate normalization parameter for the 20 sets of data in the analysis.

The data are corrected for electroweak interference and incomplete vacuum polarization corrections (see Appendix A) before the fitting procedure is applied. In the course of varying the orders of the polynomials and the number of normalization parameters, the number of free parameters varies from 12 to 44. The fit quality does not improve substantially when the number of parameters exceeds 14. The data and the result of the fit used to evaluate the central value of $\Delta\alpha_{had}^{\text{cont}}$ are shown in Fig. 3. The error bars include the point-to-point and the normalization uncertainties. The fit quality is reasonable ($\chi^2/\text{dof} = 110/100$).

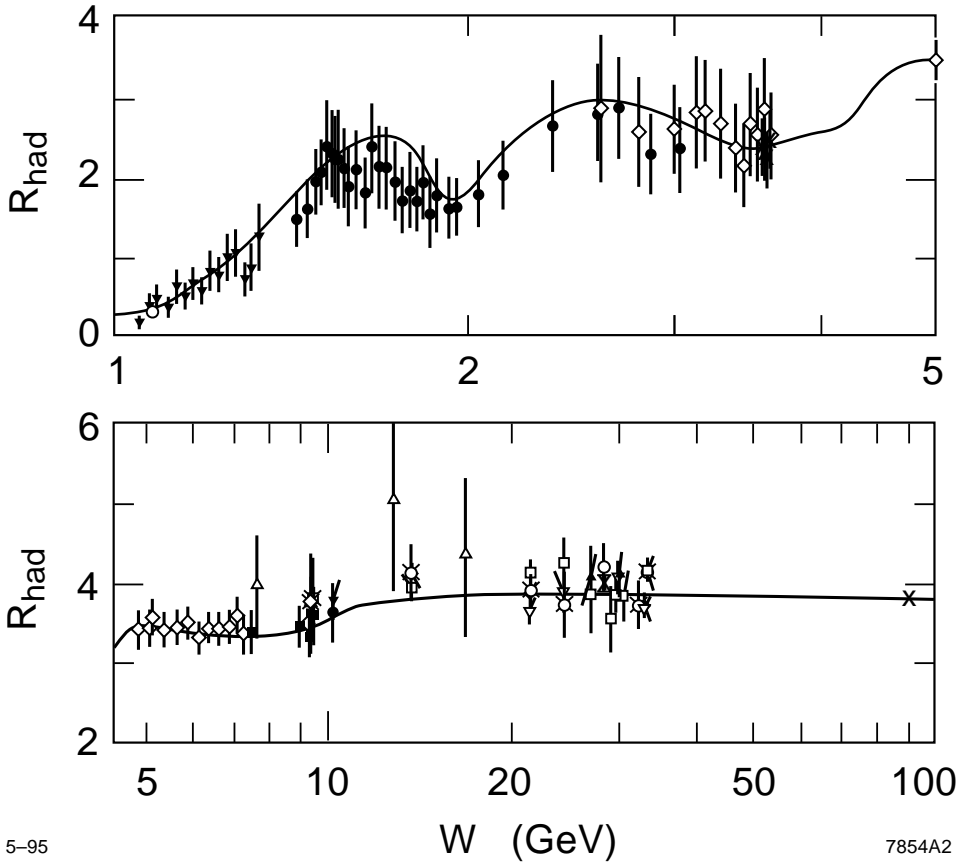


Figure 3. The continuum R_{had} measurements including normalization uncertainties. The entries in the region below charm threshold consist of a compilation of low energy exclusive cross sections [25,24,27] (solid inverted triangles) and the measurements of the $\gamma\gamma 2$ [26] (solid dots), Mark I [28] (open diamonds), DASP [29] (X's), Crystal Ball [31] (solid square), and PLUTO [30] (solid diamond) Collaborations. The entries in the region between charm and bottom thresholds are the measurements of Crystal Ball [32] (open diamonds), PLUTO [30] (open triangles), LENA [33] (solid squares), DASP [29] (diamond-X overlay), DESY-Heidelberg [36] (square-X overlay), CUSB [35] (solid dot), and CLEO [34] (solid inverted triangle) Collaborations. The entries in the region between above bottom threshold and below the Z pole are the measurements of CELLO [42] (open diamonds), PLUTO [30] (open triangles), JADE [33] (open squares), Mark-J [44] (open inverted triangles), TASSO [45] (circle-X overlay), HRS [40] (open circle), and MAC [41] (X) Collaborations. The fit used to evaluate the central value of $\Delta\alpha_{had}^{\text{cont}}$ is shown as the solid curve.

The various hypotheses for R_{fit} are used to evaluate the integral in equation (5) from $s_0 = 1 \text{ GeV}^2$ to $\infty = 10^6 \text{ GeV}^2$. Although the singularity in the integrand is formally well controlled, digital computers are famous for their inability to understand formalities. We have therefore recast equation (5) into a form which is more suitable for electronic evaluation,

$$\Delta\alpha_{had}(q^2) = \frac{\alpha_0 q^2}{3\pi} \left\{ \frac{R_{fit}(q^2)}{q^2} \ln \left[\frac{q^2 - s_0}{s_0} \right] - \int_{s_0}^{q^2 - \Delta} ds \frac{R_{fit}(s) - R_{fit}(q^2)}{s(s - q^2)} \right. \\ \left. - \frac{\partial R_{fit}}{\partial s} \Big|_{q^2} \ln \left[\frac{q^2 + \Delta}{q^2 - \Delta} \right] - \int_{q^2 + \Delta}^{\infty} ds \frac{R_{fit}(s) - R_{fit}(q^2)}{s(s - q^2)} \right\}, \quad (18)$$

where we have assumed that R_{fit} is well approximated by a linear expansion over the interval $q^2 - \Delta < s < q^2 + \Delta$ (in practice, we use $\Delta = 0.5 \text{ GeV}^2$). The evaluation of equation (18) requires that α_s be evolved to scales larger than the t-quark mass. For this purpose, the top quark mass is assumed to be 172.3 GeV which is the $\overline{\text{MS}}$ mass corresponding to a pole mass of 180 GeV.

The contribution of the hadronic continuum to $\Delta\alpha_{had}(M_Z^2)$ is found to be fairly insensitive to the form of R_{fit} and the number of normalization parameters used. The central value of $\Delta\alpha_{had}(M_Z^2)$ corresponds to the best estimate of the parameters of the function which uses: the DASP shape for the c-quark-threshold, the free-quark shape for the b-quark-threshold, the values (2,3,3) for (N_b, N_c, N_s) and four normalization parameters. The maximum deviation from this value occurs when $N_b = 1$ and four (instead of 20) normalization parameters are used (the deviation is insensitive to the choice of threshold functions). The size of the maximum deviation is taken as an estimate of the parameterization uncertainty. The experimental uncertainty given by equation (8) is found to be in excellent agreement with the estimate derived from an ensemble of 500 fluctuated data sets. The resulting contribution to $\Delta\alpha_{had}(M_Z^2)$ is

$$\Delta\alpha_{had}^{\text{cont}}(M_Z^2) = 0.022106 \pm 0.000366(\text{exp}) \pm 0.000196(\text{param}). \quad (19)$$

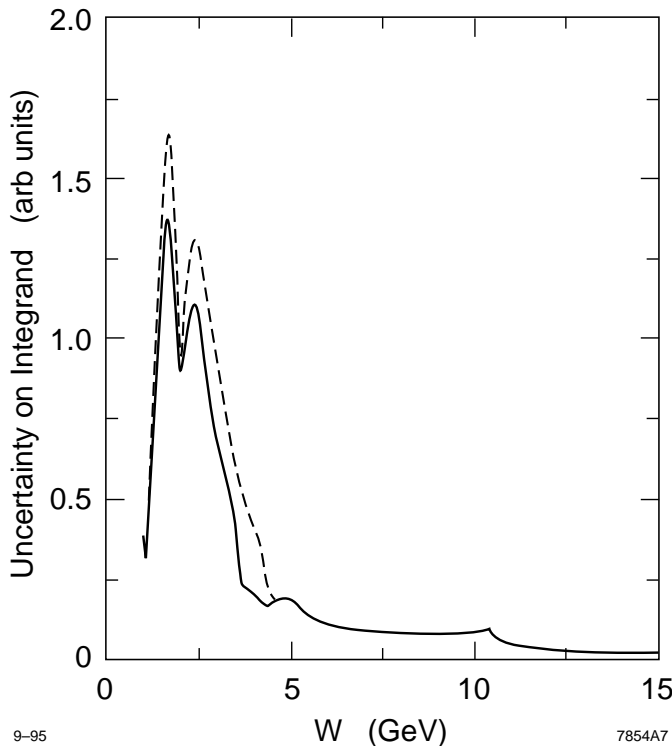


Figure 4. The uncertainty on the integrand of the dispersion integral (integrated over W rather than s) in arbitrary units. The dashed curve shows the uncertainty before the Crystal Ball data point is included in the fit and the solid curve shows the uncertainty after its inclusion.

This result differs from our previous result [9] by $+0.000678$. Most of the difference is caused by inclusion of Crystal Ball data point at 3.670 GeV ($+0.000575$). The remaining difference is due to the use of the five-flavor definition of $\Delta\alpha_{had}$ ($+0.000059$), a change in the value of $\alpha_s(M_Z^2)$ used as input (-0.000051), and the change to the unbiased fitting technique ($+0.000095$). The inclusion of the Crystal Ball point pulls the fit to somewhat larger values of R_{had} and substantially constrains the normalization in the charm threshold region. The Mark II and $\gamma\gamma 2$ data span a large energy region and constrain the shape of $R_{fit}(W)$ down to $W = 1.4$ GeV. The effect of the single precise point is therefore propagated to smaller energies. This type of effect is illustrated in Figure 1(a) and is

demonstrated in Figure 4 which displays the uncertainty on the integrand of the W -space dispersion integral in arbitrary units [48]. The uncertainty is calculated using equation (8) (with $\Delta\alpha_{had}$ replaced by R_{fit}) to estimate the uncertainty on $R_{fit}(W)$ at each energy point. The dashed curve shows the uncertainty before the Crystal Ball data point is included in the fit and the solid curve shows the uncertainty after its inclusion. Note that the overall uncertainty on $\Delta\alpha_{had}^{\text{cont}}$ is dominated by the poor precision of the data in the 1 GeV to 3.5 GeV region.

2.4 THE $\pi^+\pi^-$ AND K^+K^- FINAL STATES

The processes $e^+e^- \rightarrow \pi^+\pi^-$ and $e^+e^- \rightarrow K^+K^-$ are described by the electromagnetic form factors, $F_\pi(s)$ and $F_K(s)$, which are related to the hadronic cross section ratio R_{had} for each process as follows,

$$R_{had}^{\pi^+\pi^-}(s) = \frac{1}{4}|F_\pi(s)|^2\beta_\pi^3, \quad R_{had}^{K^+K^-}(s) = \frac{1}{4}|F_K(s)|^2\beta_K^3, \quad (20)$$

where β_π and β_K are the velocities of the final state particles in the e^+e^- center-of-mass frame. It is clear that measurements of the form factors are equivalent to measurements of R_{had} .

Measurements of the square of the pion form factor $|F_\pi|^2$ have been performed by the OLYA [12], CMD [12], TOF [14], NA7 [13], $\mu\pi$ [17], MEA [19], M2N [15], DM1 [16], and DM2 [18] Collaborations and are shown in Fig. 5. The error bars include the normalization uncertainties which range from about 2% in the region around the (dominant) ρ resonance to about 12% at $W \simeq 2$ GeV.

The data are first corrected for incomplete vacuum polarization corrections as described in Appendix A. They are then fit to a function which is a sum of the Gounaris-Sakurai form [49] used by Kinoshita, Nizic, and Okamoto [50] and three resonances,

$$F_\pi(s) = \frac{A_1 - m_\pi^2 A_2}{A_1 + A_2 q^2 + f(s)} + \sum_{n=1}^3 \frac{B_n e^{iC_n} m_n^2}{s - m_n^2 + i m_n \Gamma_n}, \quad (21)$$

where: A_1 and A_2 are free parameters; m_π is the pion mass; q and $f(s)$ are defined

as follows,

$$q \equiv \sqrt{s/4 - m_\pi^2} \\ f(s) \equiv \frac{1}{\pi} \left[m_\pi^2 - \frac{s}{3} \right] + \frac{2q^3}{\pi\sqrt{s}} \ln \left[\frac{\sqrt{s} + 2q}{2m_\pi} \right] - i \frac{q^3}{\sqrt{s}}; \quad (22)$$

and where m_n , Γ_n , B_n , and C_n are the mass, width, amplitude, and phase of each resonance. The mass and width of the first resonance are set to those of the $\omega(782)$. All other parameters (12 in total) are allowed to vary. The χ^2 function is constructed assuming that all normalization uncertainties are 100% correlated (one normalization parameter) and that the normalizations are uncorrelated (seven normalization parameters). As in the case of the continuum, the two fits give nearly identical results but the error estimate is larger when only one normalization parameter is used. The result of the single-normalization-parameter-fit is shown as a solid line in Fig. 5. The fit preferred a resonance of width 0.44 GeV at mass 1.15 GeV and a second resonance of width 0.18 GeV at mass 1.71 GeV. The fit quality is found to be good ($\chi^2/\text{dof} = 138.3/127$).

To evaluate the sensitivity of the result to the parameterization, the complete function used by the authors of Ref. 50 was also fit to the data. This function did not fit the newest (large W) data from DM2 as well as our chosen form ($\chi^2/\text{dof} = 201.5/132$). Both functions were used to evaluate equation (5) from $s = 4m_\pi^2$ to $s = 4 \text{ GeV}^2$ (where $|F_\pi|^2$ is measured to be very small). We find the $\pi^+\pi^-$ contribution to $\Delta\alpha_{\text{had}}(M_Z^2)$ to be

$$\Delta\alpha_{\text{had}}^{\pi^+\pi^-}(M_Z^2) = 0.003240 \pm 0.000057(\text{exp}) \pm 0.000169(\text{param}). \quad (23)$$

The two techniques for the estimation of the experimental uncertainty (discussed in Section 2.1) yield consistent results.

The result given in equation (23) differs from our previous result [9] by $+0.000153$. The difference is due entirely to the use of the unbiased fitting technique and represents the largest problem found with the older technique.

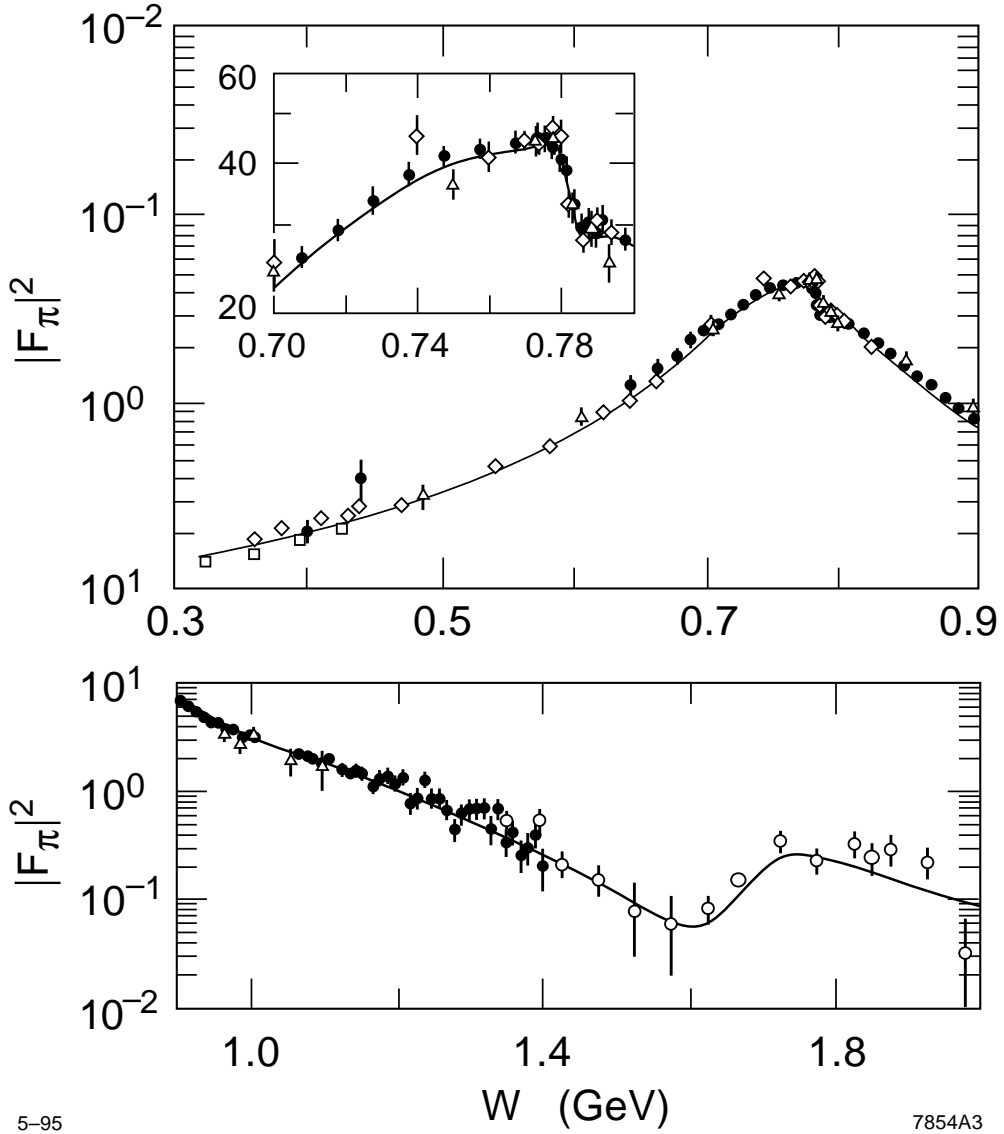


Figure 5. Measurements of $|F_\pi(W)|^2$ by the OLYA [12] (solid dots), CMD [12] (open diamonds), TOF [14] (solid triangles), NA7 [13] (open squares), $\mu\pi$ [17] (solid squares), MEA [19] (solid diamonds), DM1 [16] (open triangles), and DM2 [18] (open circles) Collaborations are compared with the best fit which is shown as a solid line. The error bars include normalization uncertainties.

Measurements of the square of the kaon form factor $|F_K|^2$ have been performed by the OLYA [20], CMD [21], MEA [19], DM1 [22], and DM2 [23] Collaborations and are shown in Fig. 6. The data span the $\phi(1020)$ resonance and continue to

$W = 1.8$ GeV where $R_{had}^{K^+K^-}$ is less than 0.01. The normalization uncertainty on the CMD measurements is 6%. The other groups do not report normalization uncertainties. Early $|F_\pi|^2$ measurements suffered from the same problem of unreported normalization uncertainties. A bit of historical research shows that the normalization uncertainties were usually not included in the point-to-point errors. We therefore arbitrarily assign a 20% systematic normalization uncertainty to all unreported cases. The data and total uncertainties are shown in Fig. 6.

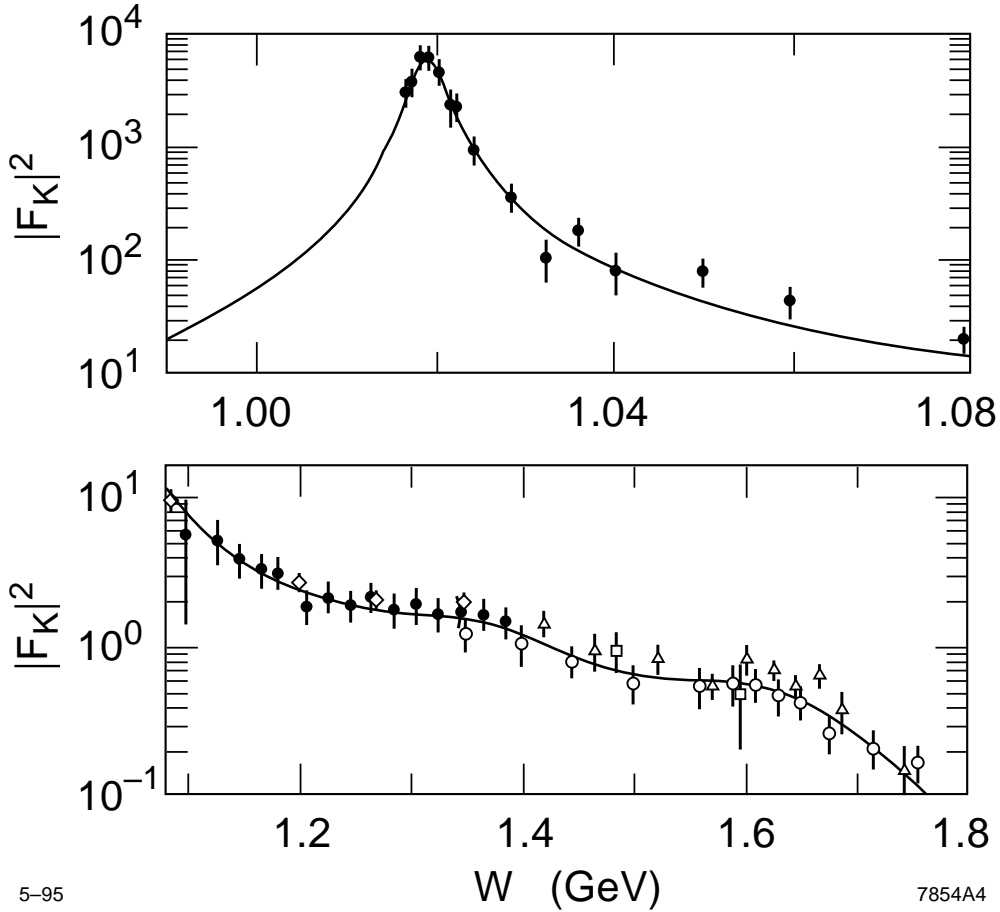


Figure 6. Measurements of $|F_K(W)|^2$ by the OLYA [20] (solid dots), CMD [21] (open diamonds), MEA [19] (open squares), DM1 [22] (open triangles), and DM2 [23] (open circles) Collaborations are compared with the best fit which is shown as a solid line. The error bars include normalization uncertainties.

The data are fit to a function which is a sum of a Breit-Wigner resonance with

an energy-dependent width for the ϕ and four resonances,

$$F_K(s) = \frac{A_1}{s - m_\phi + im_\phi\Gamma_\phi(s)} + \sum_{n=1}^4 \frac{B_n e^{iC_n}}{s - m_n^2 + im_n\Gamma_n}, \quad (24)$$

where: A_1 is the amplitude of the ϕ ; m_ϕ is the mass of the $\phi(1020)$; m_n , Γ_n , B_n , and C_n are the mass, width, amplitude, and phase of the resonances. The energy-dependent width $\Gamma_\phi(s)$ is assumed to consist of contributions from the K^+K^- , K_LK_S , and 3π final states,

$$\Gamma_\phi(s) = \Gamma_\phi^0 \left\{ \frac{\sqrt{s}}{m_\phi} \left[0.497 \frac{\beta_+^3(s)}{\beta_+^3(m_\phi^2)} + 0.347 \frac{\beta_0^3(s)}{\beta_0^3(m_\phi^2)} \right] + 0.156 G_{3\pi}^\phi(s) \right\}, \quad (25)$$

where: Γ_ϕ^0 is the nominal value [10] of the ϕ width, $\beta_+(s) = \sqrt{1 - 4m_{K^+}^2/s}$ is the velocity of the charged kaon, $\beta_0(s) = \sqrt{1 - 4m_{K^0}^2/s}$ is the velocity of the neutral kaon, and $G_{3\pi}^\phi(s)$ is a function which is normalized to unity at $s = m_\phi^2$ and is proportional to the decay rate for $\phi \rightarrow 3\pi$ assuming $\rho\pi$ dominance [51].

The masses and widths of the first two resonances were set to those of the $\rho(770)$ and $\omega(782)$. Following the procedure of Ref. 23, the amplitude ratios B_1/A_1 and B_2/A_1 were constrained to the measured values and the phases were set to zero. The mass, width, and amplitude of the ϕ were allowed to vary. The masses, widths, amplitudes, and phases of two larger mass resonances were free parameters. The χ^2 function was constructed with the assumptions that all normalization uncertainties are 100% correlated (one normalization parameter) and the normalization uncertainties are uncorrelated (five normalization parameters). The $|F_K|^2$ fit was the only instance for which the different assumptions about the correlation of the normalizations yielded noticeably different fit results. In this case, the assumption that the normalizations are uncorrelated (five normalization parameters) produced a substantially better fit to the data ($\chi^2/\text{dof} = 48.9/44$) than did the assumption that they are correlated ($\chi^2/\text{dof} = 73.6/48$). The better fit is plotted as a solid line in Fig. 6. The fit preferred a resonance of width 0.17 GeV at mass 1.35 GeV and a second resonance of width 0.24 GeV at mass 1.68 GeV.

To evaluate the sensitivity of the result to the parameterization, a second fit was performed with the amplitudes and phases of the ρ and ω allowed to vary as free parameters. No appreciable differences differences from the first pair of fits were observed. Evaluating equation (5) from $s = 4m_{K^+}^2$ to $s = 3.24 \text{ GeV}^2$, we find the K^+K^- contribution to $\Delta\alpha_{had}(M_Z^2)$ to be

$$\Delta\alpha_{had}^{K^+K^-}(M_Z^2) = 0.000356 \pm 0.000032(\text{exp}) \pm 0.000030(\text{param}) \quad (26)$$

where the parameterization uncertainty reflects the difference obtained from the two χ^2 definitions. The two techniques for the estimation of the experimental uncertainty (discussed in Section 2.1) yield consistent results in this case.

2.5 THE RESONANCES

The resonances comprise the remaining portion of the total e^+e^- cross section. The total cross section for each resonance can be represented by a relativistic Breit-Wigner form with an energy-dependent total width [52],

$$\sigma_{res}(s) = \frac{12\pi}{m} \frac{\sqrt{s}\Gamma_{ee}\Gamma_{fs}(s)}{(s - m^2)^2 + s\Gamma_{tot}^2(s)}, \quad (27)$$

where: m , Γ_{ee} , and Γ_{tot} are the mass, electronic width, and energy-dependent total width of the resonance; and Γ_{fs} is the energy-dependent width corresponding to the final states considered in the analysis. Note that the electronic widths are physical widths (not corrected for vacuum polarization effects). In order to incorporate the Breit-Wigner cross section described by equation (27) into equation (5), it must be scaled to the electromagnetic point cross section, $\sigma_{\mu\mu}(s) = 4\pi\alpha^2(s)/3s$, yielding the following expression,

$$\Delta\alpha_{had}^{res}(q^2) = \frac{\alpha_0 q^2}{4\pi^2} P \int_{4m_\pi^2}^{\infty} ds \frac{\sigma_{res}(s)}{\alpha^2(s)[q^2 - s]}, \quad (28)$$

which has the slightly unpleasant feature that it incorporates $\alpha(s)$, the quantity that we are attempting to evaluate, into the integrand. To avoid this problem, we

use the $\Delta\alpha_{had}(s)$ parameterization given in Ref. 4 to generate a first-order estimate of $\alpha(s)$ for use in equation (28). Note that equation (28) is often written with $\alpha(s)$ replaced by α_0 . This is correct only if the cross section σ_{res} is replaced by the tree-level one, $\sigma_{res}^0 = \sigma_{res} \cdot \alpha_0^2/\alpha^2(s)$. The factor $\alpha_0^2/\alpha^2(s)$ is often absorbed into equation (27) by defining the tree-level electronic width $\Gamma_{ee}^0 \equiv \Gamma_{ee} \cdot \alpha_0^2/\alpha^2(m^2)$.

Equation (28) is evaluated for the $\omega(782)$, $\phi(1020)$, ψ -family, and Υ -family resonances by performing a Simpson's rule integration over the interval $m - 60\Gamma_{tot}$ to $m + 60\Gamma_{tot}$ (the lower limit of the ω integration is the threshold for 3π decay). The energy-dependent total widths of the ψ and Υ resonances are assumed to scale as \sqrt{s} ,

$$\Gamma_{tot}(s) = \frac{\sqrt{s}}{m} \Gamma_{tot}(m), \quad (29)$$

where m is the mass of the resonance and $\Gamma_{tot}(m)$ is the nominal value of the width. All ψ and Υ final states are included in the resonance contribution [$\Gamma_{fs}(s) = \Gamma_{tot}(s)$]. The energy-dependent total width of the $\phi(1020)$ is given by equation (25). The width $\Gamma_{fs}(s)$ for the ϕ is adjusted to exclude the K^+K^- final state (discussed in Section 2.4). The energy-dependent total width of the $\omega(782)$ is given by the following expression which assumes that all final states are $\pi^+\pi^-$, $\pi^0\gamma$, or $\pi^+\pi^-\pi^0$,

$$\Gamma_\omega(s) = \Gamma_\omega^0 \left\{ \frac{\sqrt{s}}{m_\omega} \left[0.022 \frac{\beta_\pi^3(s)}{\beta_\pi^3(m_\omega^2)} + 0.085 \frac{(1 - m_\pi^2/s)^3}{(1 - m_\pi^2/m_\omega^2)^3} \right] + 0.893 G_{3\pi}^\omega(s) \right\}, \quad (30)$$

where: m_ω is the mass of the ω , Γ_ω^0 is the nominal value [10] of the ω width, $\beta_\pi(s) = \sqrt{1 - 4m_\pi^2/s}$ is the velocity of the charged pion, and $G_{3\pi}^\omega(s)$ is a function which is normalized to unity at $s = m_\omega^2$ and is proportional to the decay rate for $\omega \rightarrow 3\pi$ assuming a constant matrix element (phase space weighting). The width $\Gamma_{fs}(s)$ for the ω is adjusted to exclude the $\pi^+\pi^-$ final states which are included in the $|F_\pi|^2$ contribution.

The masses and widths used to evaluate equation (28) are taken from the 1994 Review of Particle Properties [10]. The Particle Data Group does not apply a consistent set of definitions to the parameters of all resonances. The electronic widths

of the ψ and Υ families are defined to be the physical ones and are derived from fits performed by the PDG itself. The electronic widths of the ω and ϕ resonances are determined from measurements of the total widths and electronic branching fractions B_{ee} . In both cases, the total widths are the correct physical ones. The average value of $B_{ee}(\omega)$ is dominated by peak cross section measurements of the CMD [53] and ND [54] Collaborations which are corrected (partly) for vacuum polarization effects and lead to a determination of $\Gamma_{ee}^0(\omega)$. The case of the ϕ is less clear. Of the three most precise measurements of $B_{ee}(\phi)$, those of the DM1 [55] and OLYA [56] Collaborations are not corrected for vacuum polarization effects and lead to a determination of $\Gamma_{ee}(\phi)$. The most precise measurement is a later OLYA result which has about the same precision as the combination of the two preceding results but is reported in an unpublished preprint which is no longer available for inspection. The result may (or may not) be corrected for vacuum polarization effects. We make the assumption that the RPP value of $\Gamma_{ee}(\phi)$ is the physical one. This assumption cannot be wrong by more than one half of the total vacuum polarization correction (1.6%) which we include in the uncertainty on $\Gamma_{ee}(\phi)$.

The leptonic widths are corrected for incomplete vacuum polarization correction to the normalizing cross sections (see Appendix A) before equation (28) is evaluated. The results are listed in Table 1 along with those derived in Sections 2.3 and 2.4. The experimental uncertainties are evaluated by assuming that the uncertainties on the masses, total widths, electronic widths, and relevant branching ratios are uncorrelated. The parameterization uncertainties are evaluated by repeating the calculation with a constant-width, constant-mass Breit-Wigner cross section.

2.6 FINAL RESULT

The various contributions to $\Delta\alpha_{had}(M_Z^2)$ are summarized and summed in Table 1. The resulting value is

$$\Delta\alpha_{had}(M_Z^2) = 0.02752 \pm 0.00046. \quad (31)$$

Including the leptonic contribution, we find $\alpha^{-1}(M_Z^2)$ to be,

$$\alpha^{-1}(M_Z^2) = 128.96 \pm 0.06, \quad (32)$$

where the uncertainties on the lepton masses contribute negligibly to the total uncertainty. This result differs by one of its standard deviations from the (common) result given in References 7 and 8 and it differs by 0.3 standard deviations from the result given in Reference 6. However, since the different analyses make use of many of the same inputs, the results are not independent measurements of $\Delta\alpha_{had}(M_Z^2)$ but reflect differences in assumptions and technique.

Table 1: Summary of the various contributions to $\Delta\alpha_{had}$.

Contribution	W Region (GeV)	$\Delta\alpha_{had}(M_Z^2)$	$\delta(\Delta\alpha_{had})_{exp}$	$\delta(\Delta\alpha_{had})_{param}$
Continuum	1.0- ∞	0.022106	0.000366	0.000196
$\pi^+\pi^-$	0.280-2.0	0.003240	0.000057	0.000169
K^+K^-	0.987-1.8	0.000356	0.000032	0.000030
Resonances	$\omega^{(a)}$	0.000307	0.000010	0.000003
"	$\phi^{(b)}$	0.000296	0.000012	0.000004
"	ψ (6 states)	0.001101	0.000059	0.000023
"	Υ (6 states)	0.000118	0.000005	0.000003
Total		0.02752	0.00038	0.00026

(a) Doesn't include $\pi^+\pi^-$ final states.

(b) Doesn't include K^+K^- final states.

2.7 DETAILED COMPARISON WITH REFERENCE 7

The result of Eidelman and Jegerlehner [7] (henceforth E-J) is based almost entirely upon the trapezoidal integration of locally averaged data points. Only the narrow resonances are treated parametrically. E-J have published their composite compilation of the function $R_{had}(W)$ in a series of figures and include a detailed breakdown of the contributions of various energy intervals to $\Delta\alpha_{had}(M_Z^2)$. Since the E-J compilation excludes narrow resonances, we construct the function R_{sum} to include the same final states,

$$R_{sum}(W) = R_{fit}(W) + \frac{1}{4}|F_\pi(W)|^2\beta_\pi^3 + \frac{1}{4}|F_K(W)|^2\beta_K^3 + \sum_{i=1}^5 \sigma_{res}^i(W), \quad (33)$$

where the sum includes the $\omega(782)$, $\phi(1020)$, $\psi(4040)$, $\psi(4160)$, and $\psi(4415)$ resonances. A comparison of their R_{had} compilation (R_{had}^{EJ}) with R_{sum} in the region $W = 1 - 50$ GeV is shown in Figures 7 and 8. The R_{had}^{EJ} compilation is shown as the solid curve in both figures. The dashed curve in Figure 7 shows R_{sum} before the inclusion of the Crystal Ball measurement at 3.67 GeV. The dashed curve in Figure 8 shows R_{sum} after the inclusion of the new data point. The peak of the ϕ between 1.00 GeV and 1.04 GeV is suppressed in both figures.

A comparison of Figures 7 and 8 shows the effect of the Crystal Ball measurement quite clearly. Before the point is added to the analysis, there is reasonable agreement between the functions $R_{sum}(W)$ and $R_{had}^{EJ}(W)$ in the region 1.0-1.8 GeV. Between 1.8 GeV and 3.6 GeV, R_{had}^{EJ} is generally larger than R_{sum} . After the introduction of the Crystal Ball measurement, the $\gamma\gamma 2$ measurements are renormalized to larger values and the fitting function generally exceeds the R_{had}^{EJ} compilation throughout the region.

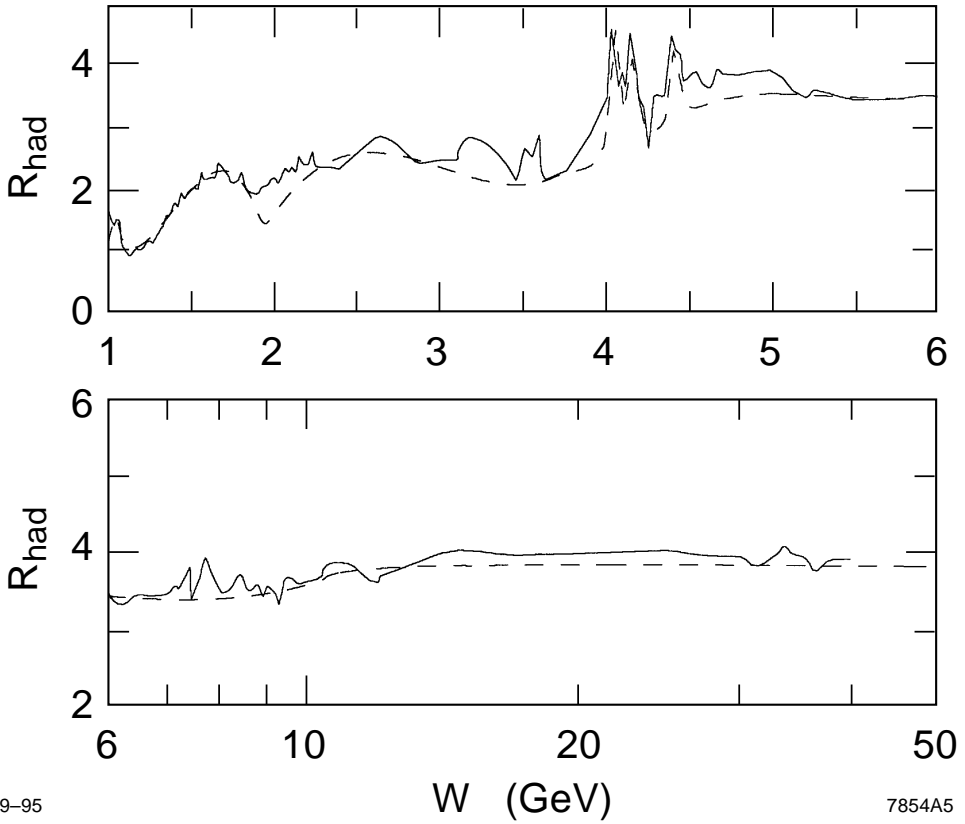


Figure 7. A comparison of our total R_{had} function (dashed curve) before the inclusion of the Crystal Ball measurement at 3.67 GeV with that from Reference 7.

The agreement between R_{sum} and R_{had}^{EJ} in the charm threshold region between 3.6 GeV and 5.0 GeV is also quite poor. The R_{sum} function follows the shape of the DASP fit to the continuum under the $\psi(4040)$, $\psi(4160)$, $\psi(4415)$ resonances and includes the resonances explicitly for comparison. The size of the continuum portion is determined at 3.6 GeV and 5.0 GeV by the most precise data in those regions (Crystal Ball data in both cases) yielding a continuous result. The R_{had}^{EJ} compilation generally exceeds R_{sum} throughout the region reflecting the fact that DASP and PLUTO generally measured large values of R_{had} in the region. The more precise Crystal Ball measurements begin at 5.0 GeV and pull the R_{had}^{EJ} function to smaller values, creating an apparent structure in the 4.4-5.0 GeV region. The apparent structure is not seen by any of the experiments that have measured the

shape and magnitude of $R_{had}(W)$ in this region and is entirely a consequence of ignoring the shape information inherent in the data (a more correct procedure would renormalize the data sets so that the integrated function was smooth and continuous in the 5-5.2 GeV region).

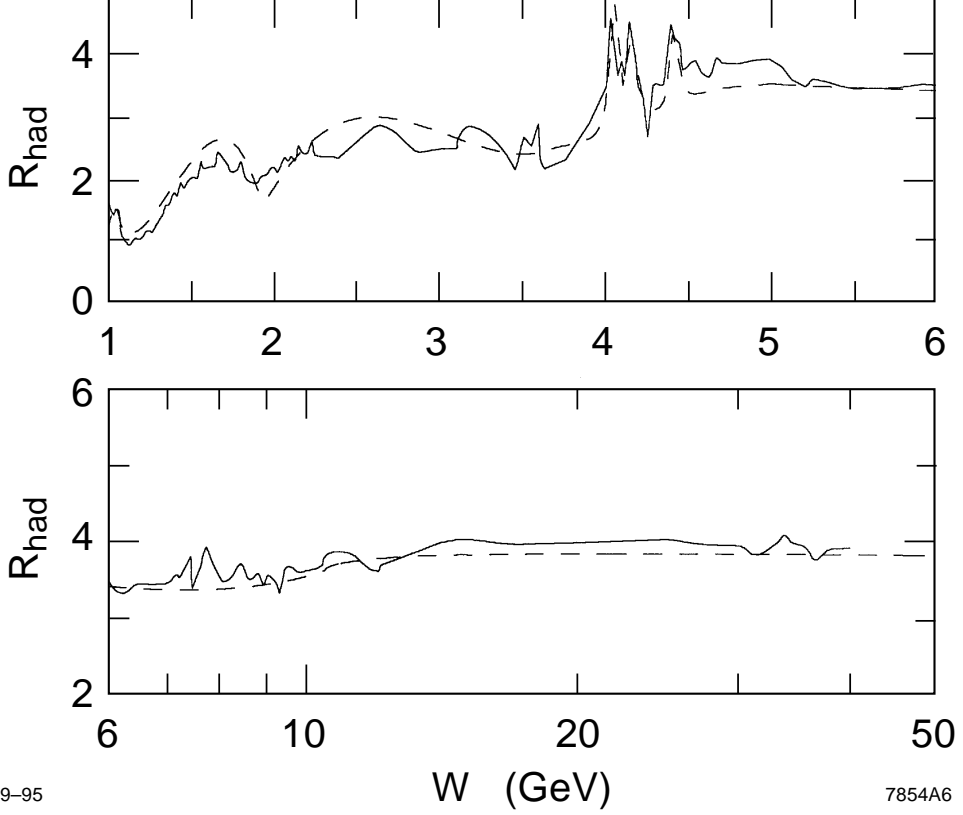


Figure 8. A comparison of our total R_{had} function (dashed curve) after the inclusion of the Crystal Ball measurement at 3.67 GeV with that from Reference 7.

In the region $W = 5 - 10$ GeV, the agreement of the R_{sum} and R_{had}^{EJ} functions is somewhat better except for some wiggles in R_{had}^{EJ} at the larger energies. Above b-threshold and below $W = 40$ GeV (where the authors of Reference 7 begin to use perturbative QCD), the R_{had}^{EJ} compilation is somewhat larger than R_{sum} reflecting the fact the the PEP/PETRA measurements of R_{had} are somewhat larger than those predicted by perturbative QCD with currently favored values of $\alpha_s(M_Z^2)$.

The differences shown qualitatively in Figure 8 are quantified in Table 2 using

the detailed breakdown scheme presented in Reference 7. The entries in square brackets are from Ref. 7 before the application of corrections for incomplete vacuum polarization correction. In Appendix A, we demonstrate that the non-application of this correction is generally a more accurate approximation than the use of the factor favored by the authors of Ref. 7. A comparison of our result with the bracketed quantities (or the means of the pairs of quantities) is probably the more relevant one. Note that our value for the contribution of $\pi^+\pi^-$ final states in the interval $W = 0.28 - 0.81$ GeV of 24.11 (in units of 10^{-4}) is somewhat smaller than the value of 26.08 given in Reference 7. The difference may be due in part to the preference of our fit for smaller values of $|F_\pi|^2$ than the central values of the OLYA measurements between 0.6 GeV and 1.0 GeV (see Fig. 5). The opposite behavior is observed when the full function used in the analysis of Kinoshita, Nizic, and Okamoto [50] is fit to the data. The large-energy tail of this function decreases with energy more steeply than do the data points. A fit to this function prefers larger values of $|F_\pi|^2$ than the central values of the OLYA measurements between 0.6 GeV and 1.0 GeV yielding a contribution to $\Delta\alpha_{had}(M_Z^2)$ of 25.39 . Excluding the influence of the steeply falling tail by restricting the fit of the KNO function to the region $W < 1.0$ GeV relaxes some of the bias and yields a $\Delta\alpha_{had}(M_Z^2)$ contribution of 24.76 . These differences are reflected in the large size of the parameterization uncertainty given in Table 1.

We conclude that the agreement of our analysis with one based almost entirely on trapezoidal integration is somewhat poorer than a comparison of the final $\Delta\alpha_{had}(M_Z^2)$ results would indicate. Part of the discrepancy is caused by the loss of shape information from multi-point measurements inherent in the averaging procedure which treats the individual measurements as independent. An associated side effect is that sparse, newer measurements influence the integrated function only over an interval between neighboring older measurements. The addition of the precise Crystal Ball point (which fixes the normalization of R_{had} over a large region in our analysis) to a trapezoidal analysis would affect only a very small region. Conversely, the trapezoidal analysis remains influenced by older measure-

ments until they are replaced by newer measurements at the same or very nearby energies. The effect of the apparent structure in the charm threshold region or the large R_{had} values from the PEP/PETRA region will persist until replaced (or influenced) by newer measurements at the same energies. The use of a continuous fitting function in our analysis allows us to interpolate between sparse but precise points. For these reasons, we do indeed “believe more in the integration of our fits than in trapezoidal integration” as noted by the authors of Ref. 7.

Table 2: Comparison of the various contributions to $\Delta\alpha_{had}(M_Z^2)$ with those published in Ref. 7 (in units of 10^{-4}). The entries in square brackets are from Ref. 7 before the application of corrections for incomplete vacuum polarization correction.

Final State	W Interval (GeV)	This Work	Reference 7
ρ	0.28-0.81	24.11	26.08 [26.23]
ω	0.42-0.81	2.87	2.93 [2.96]
ϕ	1.00-1.04	5.03	5.08 [5.15]
J/ψ		11.01	11.34 [11.93]
Υ		1.18	1.18 [1.27]
all hadrons	0.81-1.40	13.55	13.83 [13.99]
all hadrons	1.40-3.10	30.42	27.62 [28.23]
all hadrons	3.10-3.60	5.62	5.82 [5.98]
all hadrons	3.60-9.46	48.16	50.60 [50.50]
all hadrons	9.46-40.0	90.67	93.07
all hadrons	$40.0-\infty$	42.64	42.82
Total		275.2	280.4 [282.1]

3. Conclusions

We have reevaluated the hadronic part of the electromagnetic vacuum expectation value using the standard dispersion integral approach that utilizes the hadronic cross section measured in e^+e^- experiments as input. Previous analyses are based upon point-by-point trapezoidal integration which does not treat experimental errors in an optimal way. We use a technique that weights the experimental inputs by their stated uncertainties, includes correlations, and incorporates some refinements. We find the five-flavor hadronic contribution to the fractional change in the electromagnetic coupling constant at $q^2 = M_Z^2$, $\Delta\alpha(M_Z^2)$, to be 0.02752 ± 0.00046 , which leads to a value of the electromagnetic coupling constant, $\alpha^{-1}(M_Z^2) = 128.96 \pm 0.06$.

The current generation of Z -pole asymmetry measurements have already determined the effective weak mixing angle $\sin^2\theta_W^{\text{eff}}$ to a precision of ± 0.00028 [57]. Future measurements may improve the determination to the ± 0.00020 level. This is comparable to the theoretical uncertainty of ± 0.00016 which follows from the ± 0.06 uncertainty on $\alpha^{-1}(M_Z^2)$. It is clear that improved understanding of $\alpha(M_Z^2)$ is desirable and it is also clear (from Figure 4) that improved understanding requires improved data in the $W = 1 - 5$ GeV region. Additionally, the differences with the trapezoidal approach noted in Section 2.7 stem from questions dealing with the optimal use of rather poor quality data. Improved data will tend to make these issues less important. Among the active experimental programs of the world, only the BES Collaboration at the Beijing Electron Positron Collider is positioned to make improved measurements of R_{had} in the region $W = 2 - 5$ GeV. They are urged to include them in their long term planning.

Acknowledgements:

This work was originally motivated by the Long Term Planning Study organized by the Division of Particles and Fields of the American Physical Society. The author would like to thank Michael Peskin for his useful discussions, technical advice, and comments on this manuscript. The author would also like to thank Tatsu Takeuchi and Bill Lockman for pointing out the existence of References 11 and 31, respectively. This work was supported by Department of Energy Contract No. DE-AC03-76SF00515.

4. Appendix A: Vacuum Polarization Corrections

4.1 CORRECTIONS TO R_{had}

The quantity R_{had} is the ratio of s-channel cross sections and can be written as follows,

$$R_{had} \equiv \frac{\sigma_{had}(s)}{\sigma_{\mu\mu}(s)} = \frac{\sigma_{had}^0(s)}{\sigma_{\mu\mu}^0(s)}, \quad (34)$$

where the tree-level cross sections $\sigma^0(s)$ are related to the physical ones (already corrected for initial state radiation) by the simple expression, $\sigma^0(s) = \sigma(s)\alpha_0^2/\alpha^2(s)$. Since radiative corrections calculations combine external photonic corrections and virtual corrections, it is more straightforward for experiments to extract $\sigma_{had}^0(s)$ from their data than it is to extract $\sigma_{had}(s)$. Note that $\sigma_{\mu\mu}^0(s)$ is a simple numerical constant which is applied to the measured cross section after radiative corrections.

In Reference 7, Eidelman and Jegerlehner point out that many of the earlier measurements of R_{had} , $|F_\pi|^2$, and $|F_K|^2$ were corrected for leptonic vacuum polarization effects but were not corrected for hadronic vacuum polarization effects. To rectify this problem, they make the assumption that individual experiments

directly measure hadronic cross sections and apply the factor,

$$r_c^{EJ} = [1 + 2\Delta\alpha_\ell(s)] \frac{\alpha_0^2}{\alpha^2(s)}, \quad (35)$$

to all measurements of R_{had} , $|F_\pi|^2$, and $|F_K|^2$ below the $J\psi$ and to the Mark I measurements below charm threshold.

Unfortunately, the integrated luminosity for each measurement must be determined from the measurement of an additional physical process. Thus, experiments rarely measure cross sections directly but nearly always measure *the ratios of cross sections*. In this case, the measured value of R_{had} (or $|F|^2\beta^3/4$) is determined from the ratio of the number of observed hadronic events N_{had} to the number of observed normalizing events N_{norm} ,

$$R_{had} = \frac{N_{had}(1 + \delta_{rc})}{N_{norm}\varepsilon} \cdot \frac{\sigma_{norm}(s)}{\sigma_{\mu\mu}^0(s)}, \quad (36)$$

where δ_{rc} incorporates all radiative corrections to the hadronic yield, ε is the efficiency-acceptance product for hadronic events, and σ_{norm} is the physical cross section for the normalizing events (including all radiative effects) integrated over the acceptance used for the luminosity measurement. We note that the incomplete application of vacuum polarization corrections is a problem that applies to both the hadronic and normalizing cross sections. In this case, the actual correction should be

$$r_c = \frac{\alpha_\ell^2(s)}{\alpha^2(s)} \cdot \frac{\sigma_{norm}(s)}{\sigma_{norm}^\ell(s)} \simeq \frac{\alpha_0^2[1 + 2\Delta\alpha_\ell(s)]}{\alpha^2(s)} \cdot \frac{\sigma_{norm}(s)}{\sigma_{norm}^\ell(s)}, \quad (37)$$

where $\alpha_\ell(s)$ and $\sigma_{norm}^\ell(s)$ incorporate leptonic vacuum polarization corrections only. The difference between the two right-hand terms involves the (numerically insignificant) question of whether the original vacuum polarization corrections were performed to all orders or to first order only.

All of the early measurements of R_{had} , $|F_\pi|^2$, and $|F_K|^2$ are normalized to the number of lepton pairs observed in some portion of each apparatus. Most of the

experiments did not have (or did not use) small-angle Bhabha scattering luminosity monitors but relied instead upon large-angle lepton pairs observed in the central region of each detector. The combination of the leptonic final states and geometric acceptance used by the major experiments is summarized in Table 3. Several experiments use muon pairs to normalize their results. Since the vacuum polarization corrections to s-channel processes can be factorized (see equation (34)), the correction factor given by equation (37) is identically 1. The remaining experiments use a combination of e^+e^- and $\mu^+\mu^-$ events or e^+e^- events alone to normalize their results. The electron-pair final states are produced by the sum of s- and t-channel subprocesses. The vacuum polarization corrections to the dominant t-channel contributions are proportional to $\alpha^2(-t)$. Since the t-channel contribution dominates the Bhabha cross section, the correction factor r_c is given roughly by the following expression,

$$r_c \sim \frac{\alpha^2(-t)}{\alpha^2(s)} \cdot \frac{\alpha_\ell^2(s)}{\alpha_\ell^2(-t)}. \quad (38)$$

The key point in this discussion is that the dependence of $\alpha(q^2)$ upon the scale q^2 is logarithmic and the magnitude of $-t$ at the large angles used by most of the experiments is comparable to s (typically, $-t/s = 0.2 \rightarrow 0.4$). For this $-t$ range, the first ratio in equation (38) is typically a few percent less than unity and the second ratio is a few percent larger than unity. The net correction is therefore quite small. A complete calculation of the correction factor r_c for requires that all luminosity event selection criteria be incorporated into complete calculations of σ_{norm} and σ_ℓ^{norm} (incorporating all radiative corrections). Rather than undertake such an arduous procedure, we estimate the size of the correction from a simplified calculation which accounts for vacuum polarization effects and approximate angular acceptance. The estimate uses the low energy parameterization of $\Delta\alpha_{had}$ found in Ref. 4. The results of this estimate are listed in Table 3 along with the correction advocated by the authors of Ref. 7. Note that the corrections to the pseudoscalar form factors are estimated assuming that the original leptonic vacuum polarization corrections included electron and muon contributions. The corrections to the R_{had}

measurements are estimated assuming that the original corrections included only the electron contribution.

Table 3: Summary of the incomplete vacuum polarization correction factor r_c and that of Ref. 7, r_c^{EJ} .

Exp.	Meas.	Norm.	$ \cos(\theta) $	W (GeV)	r_c	r_c^{EJ}
NA7 [13]	$ F_\pi ^2$	$\mu\mu$	$-.875 \rightarrow .997^{(a)}$	0.320 0.422	1.0000 1.0000	0.9982 0.9972
OLYA [12,20]	$ F_\pi ^2, F_K ^2$	$ee + \mu\mu$	<0.71	0.400 1.397	0.9984 0.9952	0.9974 0.9893
CMD [12,21]	$ F_\pi ^2, F_K ^2$	$ee + \mu\mu$	<0.60	0.360 0.820	0.9988 0.9970	0.9978 0.9934
TOF [14]	$ F_\pi ^2$	$ee + \mu\mu$	<0.24	0.400 0.460	0.9990 0.9988	0.9974 0.9968
$\mu\pi$ [17]	$ F_\pi ^2$	ee	<0.61	1.250 1.520	0.9958 0.9955	0.9902 0.9886
MEA [19]	$ F_\pi ^2, F_K ^2$	ee $\mu\mu$	<0.77	1.6 1.43	0.9941 1.0000	0.9826 0.9838
DM1 [16,22]	$ F_\pi ^2, F_K ^2$	ee	<0.50	0.480 2.060	0.9983 0.9960	0.9966 0.9860
DM2 [18,23]	$ F_\pi ^2, F_K ^2$	$\mu\mu$	<0.87	1.350 2.400	1.0000 1.0000	0.9896 0.9848
$\gamma\gamma 2$ [26]	R_{had}	ee	<0.64	1.42 3.09	0.9933 0.9935	0.9839 0.9757
Mark I [28]	R_{had}	ee	<0.60	2.60 3.65	0.9936 0.9958	0.9772 0.9756
DASP [29]	R_{had}	ee	$<0.71^{(b)}$	3.6	0.9946	1.0000
PLUTO [30]	R_{had}	ee	$0.9816 \rightarrow 0.9977$	3.6	0.9756	1.0000
CMD [53]	$\Gamma_{ee}^0(\omega)$	$ee + \mu\mu$	<0.60	0.782	0.9971	0.9904
ND [54]	$\Gamma_{ee}^0(\omega)$	ee	<0.65	0.782	0.9942	0.9904

(a) Interval in $\cos\theta$.

(b) Used small-angle e^+e^- events normalized to this large angle region.

The reader should note several things. The corrections to the R_{had} , $|F_\pi|^2$, and

$|F_K|^2$ measurements are always a factor of seven or more smaller than systematic normalization uncertainties associated with the measurements. In all cases, the correction applied by the authors of Ref. 7 overestimates the true size of the correction. This overestimate is small where the correction is small but becomes significant at larger energies where the Eidelman-Jegerlehner correction exceeds 1%. In this region, the non-application of the correction ($r_c = 1.0$) is a better approximation than the one used by the authors of Ref. 7. The Eidelman-Jegerlehner analysis did not correct the hadronic continuum measurements of the DASP and PLUTO Collaborations at charm threshold although it appears that neither group applied hadronic vacuum polarization corrections [58]. The normalization DASP measurements was determined from the total number of large-angle Bhabha scattering events and is subject to a small correction. The PLUTO experiment normalized its measurements with a small-angle luminosity monitor which sampled a region of small $-t$. The cancellation of the vacuum polarization corrections is correspondingly smaller and the correction is larger.

4.2 CORRECTIONS TO RESONANCE PARAMETERS

The Breit-Wigner cross section used in Section 2.5 to calculate the resonant contribution to $\Delta\alpha_{had}(M_Z^2)$ requires the mass, total width, and electronic width of each resonance as input. The electronic widths Γ_{ee} are defined to be physical quantities (not corrected for vacuum polarization effects) and differ from the tree-level quantities Γ_{ee}^0 that have been used often in the past. The electronic widths for narrow and broad resonances are determined by different techniques but are always proportional to the peak hadronic cross section of the resonance (measured in e^+e^- collisions) or to the measured energy-integral of the hadronic cross section (taken over the resonance),

$$\Gamma_{ee} \propto \frac{N_{had}(1 + \delta'_{rc})}{N_{norm}\varepsilon} \cdot \sigma_{norm}(s), \quad (39)$$

where all quantities are defined in equation (36) except for δ'_{rc} which accounts for radiative corrections to the hadronic yield but excludes vacuum polarization

corrections. The inclusion of vacuum polarization corrections into δ'_{rc} ($\delta'_{rc} \rightarrow \delta_{rc}$) yields a measurement of the tree-level quantity Γ_{ee}^0 .

As in the case of the cross section and form factor measurements, many of the older measurements of the electronic widths were not corrected for hadronic vacuum polarization effects. It is clear that measurements of Γ_{ee}^0 must be corrected by the same correction factor r_c defined in equation (37). However, for measurements of Γ_{ee} , vacuum polarization corrections to the hadronic yield are not applied and the appropriate correction factor g_c pertains to the normalizing cross section only,

$$g_c = \frac{\sigma_{norm}(s)}{\sigma_{norm}^\ell(s)}. \quad (40)$$

As was discussed in Section 2.5, the Review of Particle Properties lists physical widths for the ψ - and Υ -family resonances as derived from their own fitting procedure. The electronic width of the $\phi(1020)$ is either the physical value or an average of the tree-level and physical values and is assumed to be the physical one. The oldest measurements of these quantities were corrected for electron vacuum polarization effects only and require the application of the additional correction factor g_c . Estimates of this factor are listed in Table 4 for measurements of the ϕ , $J/\psi(1S)$, and $J/\psi(2S)$ electronic widths. The weighted average of the ϕ correction factors is applied to the PDG value of $\Gamma_{ee}(\phi)$. The corrections to the ψ -family measurements are quite small if the original measurement was normalized to small-angle Bhabha scattering and can be as large as 2% if the large angle cross section was used as a normalization. Unfortunately, since the quoted electronic widths are derived from global fits, it is difficult to estimate the effect on the final value of Γ_{ee} . Therefore, we do not apply any corrections to the electronic widths of the ψ -family but we do inflate the uncertainties on Γ_{ee} by the size of the largest correction.

Unlike the other resonances, the electronic width of the $\omega(782)$ listed in the Review of Particle Properties is the tree-level one. We therefore apply the weighted average of the correction factors r_c listed in Table 3 for the dominant CMD and ND measurements.

Table 4: Summary of the incomplete vacuum polarization correction factor g_c .

Exp.	Res.	Norm.	$ \cos(\theta) $	g_c
DM1 [55]	$\phi(1020)$	ee	<0.50	1.0071
OLYA [56]	$\phi(1020)$	ee	<0.71	1.0052
Mark I [59]	$J/\psi(1S)$	ee	$0.9997 \rightarrow 0.9999$	1.0000
$\gamma\gamma 2$ [60]	$J/\psi(1S)$	ee	$0.9945 \rightarrow 0.9986$	1.0002
MEA [61]	$J/\psi(1S)$	ee	<0.77	1.0158
DASP [62]	$J/\psi(1S)$	ee	<0.71	1.0169
Mark I [63]	$J/\psi(2S)$	ee	<0.60	1.0204
DASP [62]	$J/\psi(2S)$	ee	<0.71	1.0189

REFERENCES

- [1] N. Cabibbo and R. Gatto, *Phys. Rev.* **124**, 1577 (1961).
- [2] See G. Burgers and W. Hollik, CERN-TH-5131/88, August 1988, and CERN 88-06, September 1988.
- [3] F.A. Berends and G.J. Komen, *Phys. Lett.* **63B**, 432 (1976); F. Jegerlehner, *Z. Phys.* **C32**, 195 and 425 (1986); B.W. Lynn, G. Penso, and C. Verzegnassi, *Phys. Rev.* **D35**, 42 (1987).
- [4] H. Burkhardt, F. Jegerlehner, G. Penso, and C. Verzegnassi, *Z. Phys.* **C43**, 497 (1989).
- [5] F. Jegerlehner, *Progress in Particle and Nuclear Physics*, Vol 27, ed. A. Faessler, Pergamon Press, Oxford 1991, p. 32; F. Jegerlehner, *Proceedings of the Theoretical Advanced Study Institute in Elementary Particle Physics*, Boulder, 1990, ed. M. Cvetic and P. Langacker, World Scientific, Teaneck N.J. 1991, p. 476.
- [6] A.D. Martin and D. Zeppenfeld, *Phys. Lett.* **B345**, 558 (1995).

- [7] S. Eidelman and F. Jegerlehner, PSI-PR-95-1, BudkerINP 95-5, January 1995.
- [8] H. Burkhardt and B. Pietrzyk, PSI-PR-95-1, LAPP-EXP-95.05, June 1995.
- [9] M.L. Swartz, SLAC-PUB-6710, December 1994, hep-ph 9411353.
- [10] Review of Particle Properties: L. Montanet, *et al.*, *Phys. Rev.* **D50**, 1173 (1994).
- [11] See G. D'Agostini, *Nucl. Inst. Meth.* **A346**, 306 (1994) for a good discussion of this effect.
- [12] CMD and OLYA Collaborations: L.M. Barkov, *et al.*, *Nucl. Phys.* **B256**, 365 (1985).
- [13] NA7 Collaboration: S. Amendolia, *et al.*, *Phys. Lett.* **B138**, 454 (1984).
- [14] TOF Collaboration: I.B. Vasserman, *et al.*, *Sov. J. Nucl. Phys.* **33**, 709 (1981).
- [15] M2N Collaboration: G. Cosme, *et al.*, *Phys. Rev. Lett.* **48**, 906 (1982).
- [16] DM1 Collaboration: A. Quenzer, *et al.*, *Phys. Lett.* **76B**, 512 (1978).
- [17] $\mu\pi$ Collaboration: G. Barbiellini, *et al.*, *Nuovo Cim. Lett.* **6**, 557 (1973).
- [18] DM2 Collaboration: D. Bisello, *et al.*, *Phys. Lett.* **220B**, 321 (1989).
- [19] MEA Collaboration: B. Esposito, *et al.*, *Phys. Lett.* **67B**, 239 (1977); B. Esposito, *et al.*, *Nuovo Cim. Lett.* **28**, 337 (1980).
- [20] OLYA Collaboration: P.M. Ivanov, *et al.*, *Phys. Lett.* **107B**, 297 (1981).
- [21] CMD Collaboration: G.V. Anikin, *et al.*, IYF-83-85, August 1983.
- [22] DM1 Collaboration: B. Delcourt, *et al.*, *Phys. Lett.* **99B**, 257 (1981); G. Grosdidier, *et al.*, LAL 80-35.
- [23] DM2 Collaboration: D. Bisello, *et al.*, *Z. Phys.* **C39**, 13 (1988).
- [24] G. Parrou, *et al.*, *Phys. Lett.* **63B**, 357 (1976).

- [25] G. Cosme, *et al.*, *Phys. Lett.* **63B**, 349 (1976); L.M. Kurdadze, *et al.*, *JETP Lett.* **43**, 643 (1986); L.M. Kurdadze, *et al.*, *JETP Lett.* **47**, 512 (1988).
- [26] $\gamma\gamma 2$ Collaboration: C. Bacci, *et al.*, *Phys. Lett.* **86B**, 234 (1979).
- [27] V.A. Sidorov, *Proceedings of the XVIIIth Conference on High Energy Physics*, ed. N.N. Bogolubov, Tbilisi, 1976.
- [28] MARK I collaboration: J.L. Siegrist, *et al.*, *Phys. Rev.* **D26**, 969 (1982); J.L. Siegrist, SLAC-Report No. 225, October 1979.
- [29] DASP Collaboration: R. Brandelik, *et al.*, *Phys. Lett.* **76B**, 361 (1978); R. Brandelik, *et al.*, *Z. Phys.* **C1**, 233 (1979); H. Albrecht, *et al.*, *Phys. Lett.* **116B**, 383 (1982).
- [30] PLUTO Collaboration: J. Burmeister, *et al.*, *Phys. Lett.* **66B**, 395 (1977); Ch. Berger, *et al.*, *Phys. Lett.* **81B**, 410 (1979).
- [31] Crystal Ball Collaboration: A. Osterheld, *et al.*, SLAC-PUB-4160, December 1986.
- [32] Crystal Ball Collaboration: Z. Jakubowski, *et al.*, *Z. Phys.* **C40**, 49 (1988); C. Edwards, *et al.*, SLAC-PUB-5160, January 1990.
- [33] LENA Collaboration: B. Niczyporuk, *et al.*, *Z. Phys.* **C15**, 299 (1982).
- [34] CLEO Collaboration: R. Giles, *et al.*, *Phys. Rev.* **D29**, 1285 (1984).
- [35] CUSB Collaboration: E. Rice, *et al.*, *Phys. Rev. Lett.* **48**, 906 (1982).
- [36] DESY-Heidelberg Collaboration: P. Bock, *et al.*, *Z. Phys.* **C6**, 125 (1980).
- [37] K.G. Chetyrkin and J.H. Kuhn, TTP-94-12, September 1994.
- [38] P. Burrows and Y. Ohnishi, private communication.
- [39] T. Sjöstrand, CERN-TH-6488-92, May 1992.
- [40] HRS Collaboration: D. Bender, *et al.*, *Phys. Rev.* **D31**, 1 (1985).
- [41] MAC Collaboration: E. Fernandez, *et al.*, *Phys. Rev.* **D31**, 1537 (1985).

- [42] CELLO Collaboration: H.-J. Behrend, *et al.*, *Phys. Lett.* **B183**, 407 (1987).
- [43] JADE Collaboration: W. Bartel, *et al.*, *Phys. Lett.* **129B**, 145 (1983); *Phys. Lett.* **B160**, 337 (1985); B. Naroska, *et al.*, *Phys. Rept.* **148**, 67 (1987).
- [44] MARK J Collaboration: B. Adeva, *et al.*, *Phys. Rev.* **D34**, 681 (1986).
- [45] TASSO Collaboration: R. Brandelik, *et al.*, *Phys. Lett.* **113B**, 499 (1982); M. Althoff, *et al.*, *Phys. Lett.* **B138**, 441 (1984).
- [46] S.G. Gorishny, A.L. Kataev, and S.A. Larin, *Phys. Lett.* **B259**, 144 (1991); L.R. Surgladze, M.A. Samuel, *Phys. Rev. Lett.* **66**, 560 (1991); Erratum: *ibid*, 2416.
- [47] See Ref. 10 and errata.
- [48] The W -space integrand $I'(W)$ is related to the s -space integrand $I(s)$ by the following simple expression $I'(W) = 2WI(W^2)$
- [49] G.J. Gounaris and J.J. Sakurai, *Phys. Rev. Lett.* **21**, 244 (1968).
- [50] T. Kinoshita, B. Nizic and Y. Okamoto, *Phys. Rev.* **D31**, 2108 (1985).
- [51] The form of the interaction Lagrangian for two vector fields (field tensors $F_1^{\mu\nu}$ and $F_2^{\mu\nu}$) and a pseudoscalar field ϕ is assumed to be $\mathcal{L} \sim F_1^{\mu\nu} \tilde{F}_{2\mu\nu} \phi / m_1$ where m_1 is the mass of the parent particle.
- [52] This form follows from the assumption that the resonance adds an imaginary part to the photon propagator $\text{Im}\Pi_{\gamma\gamma}(s) = -\sqrt{s}\Gamma_{tot}(s)$ and from the inclusion of final state phase space factors into the cross section. This form should be a better approximation near threshold which is included in the range of integration for the ϕ and ω resonances.
- [53] L.M. Barkov, *et al.*, *JETP Lett.* **46**, 164 (1987).
- [54] S.I. Dolinsky, *et al.*, *Z. Phys.* **C42**, 511 (1989).
- [55] DM1 Collaboration: G. Parrou, *et al.*, *Phys. Lett.* **63B**, 357 (1976).
- [56] OLYA Collaboration: A.D. Bukin, *et al.*, *Sov. J. Nucl. Phys.* **27**, 516 (1978).

- [57] See the presentation of A. Olshevski at the 1995 International Europhysics Conference on High Energy Physics, Brussels, Belgium.
- [58] The original work of Berends and Komen [3] in 1976 was not integrated into a radiative corrections code until the work of F.A. Berends and R. Kleiss, *Nucl. Phys.* **B178**, 141 (1981). The 1978 DASP measurement [29] explicitly states that the radiative corrections of G. Bonneau and F. Martin, *Nucl. Phys.*, **B27**, 381 (1971) were applied. The 1977 PLUTO measurement [30] merely states that radiative corrections were applied.
- [59] Mark I Collaboration: A.M. Boyarski, *et al.*, *Phys. Rev. Lett.* **34**, 1357 (1975).
- [60] $\gamma\gamma$ 2 Collaboration: R. Baldini-Celio, *et al.*, *Phys. Lett.* **58B**, 471 (1975).
- [61] MEA Collaboration: B Esposito, *et al.*, *Nuovo Cimento Lett.* **14**, 73 (1975).
- [62] DASP Collaboration: R. Brandelik, *et al.*, *Z. Phys.* **C1**, 233 (1979).
- [63] Mark I Collaboration: V. Lüth, *et al.*, *Phys. Rev. Lett.* **35**, 1124 (1975).